EES Solar

REVIEW

View Article Online
View Journal | View Issue

Cite this: *EES Sol.*, 2025, **1**, 482

Recent advances in polyoxometalates for photocatalytic carbon dioxide reduction

Guifen Li,†[a] Zheyu Wei,†[b] Yanru Shi,[c] Ruirui Zhang,[a] Xiangyi Kong,[a] Rui Ren,[a] Yafu Wang,[a] Sitan Li,[a] Yongge Wei *[b] and Jiangwei Zhang *[abcde]

With the growing global demand for energy and the increasingly serious problem of environmental pollution, the search for clean and sustainable methods of energy conversion and storage has become a hot topic in current scientific research and technology development. Photocatalytic carbon dioxide reduction (PCR) has attracted much attention in recent years as a technology capable of converting solar energy into chemical energy while achieving carbon cycling and mitigating the greenhouse effect. PCR offers the ability to convert solar energy into chemical energy through an environmentally friendly and efficient process, while promoting energy storage and carbon reduction, an innovation that has great potential to alleviate energy shortages and ameliorate environmental degradation. Polyoxometalates (POMs) show great potential for photocatalytic CO_2 reduction applications due to their unique structural properties, excellent redox capacity and tunable light absorption. This paper reviews the research progress of polyoxometalates in photocatalytic carbon dioxide reduction, including the basic properties of POMs, synthesis methods, the mechanism of photocatalytic carbon dioxide reduction, design and synthesis of POM-based catalysts, optimisation of their performance, and practical applications. There has now been a steady increase in publications and cited literature in this research area over the past decade. However, despite the growing literature, a comprehensive and in-depth review of the modification strategies, theoretical foundations, physicochemical properties and atomic level understanding of POM materials is still rare. The aim of this paper is to provide a theoretical framework for the development and refinement of POM materials in the field of photocatalytic CO_2 reduction.

Received 7th March 2025
Accepted 17th May 2025

DOI: 10.1039/d5el00026b

rsc.li/EESSolar

Broader context

In this paper, the research progress of polyoxometalates in photocatalytic carbon dioxide reduction is described in detail, including the basic characteristics of polyoxometalates, synthesis methods, the mechanism of photocatalytic carbon dioxide reduction, the design and synthesis of polyoxometalate-based catalysts, and the performance optimization and research progress of various polyoxometalate-based composites. We aim to provide valuable insights to facilitate further research on polyoxometalates in photocatalytic carbon dioxide reduction.

1. Introduction

Human civilisation and the rapid development of the global economy have become increasingly dependent on fossil fuels. It is predicted that by 2050, more than 80% of global energy consumption will come from fossil fuels.[1,2] More and more carbon dioxide emissions are causing the concentration of carbon dioxide in the atmosphere to increase every year, and high atmospheric CO_2 concentrations are widely recognised as being associated with global environmental problems.[3] Therefore, the conversion of large quantities of CO_2 into higher-value chemicals and fuels (*e.g.*, CO, CH_4, HCOOH, C_2H_4, C_2H_6) represents a highly viable environmental strategy for CO_2 emission reduction.[4]

The main methods for CO_2 reduction are electrocatalysis, thermocatalysis, and photocatalysis.[5–7] The electrochemical reduction of CO_2 takes place in a complex environment. In acidic electrolytes, the hydrogen precipitation reaction (HER) is more likely to occur, strongly competing with the CO_2RR, leading to a decrease in CO_2 reduction efficiency.[8,9] Many catalysts tend to dissolve or corrode in acidic environments, leading to decreased activity and shorter lifetimes. Moreover, in

[a]College of Energy Material and Chemistry, Inner Mongolia Key Laboratory of Low Carbon Catalysis, Inner Mongolia University, Hohhot 010021, P. R. China. E-mail: jwz@imu.edu.cn
[b]Department of Chemistry, Tsinghua University, Beijing, 100084, China. E-mail: yonggewei@mail.tsinghua.edu.cn; zjw11@tsinghua.org.cn
[c]Inner Mongolia Academy of Science and Technology, Hohhot 010021, P. R. China
[d]Key Laboratory of Advanced Energy Materials Chemistry, Nankai University, Tianjin 300071, P. R. China
[e]Ordos Laboratory, Ordos 017000, P. R. China
† These authors contributed equally.

an acidic environment, the product distribution of the CO_2RR is complex, making it difficult to control the generation of target products. Neutral electrolytes have weak buffering capacity, a slow reaction rate and poor product selectivity. Moreover, neutral electrolytes have low ionic conductivity and may require higher concentrations of electrolytes to maintain current density, but this may increase cost and introduce side reactions. In alkaline electrolytes, CO_2 reacts with OH^- to form carbonates (*e.g.*, CO_3^{2-} or HCO_3^-), and OH^- is constantly consumed, requiring frequent replenishment or replacement of the electrolyte and also leading to a lower concentration of CO_2 in the electrolyte and limiting reactant availability. Carbonates may be deposited on the catalyst surface, resulting in the active sites being covered and reducing the catalytic efficiency. Meanwhile, the thermocatalytic reduction of CO_2 requires high temperatures, which not only increase energy consumption but also reduce the quantum efficiency of the catalyst.[10] Photoelectrocatalytic CO_2 reduction technology[11] faces three primary challenges: firstly, the difficulty in achieving synergistic optimization among light absorption efficiency, charge separation efficiency, and catalytic activity results in generally low overall energy conversion efficiency (<2%). Secondly, poor catalyst stability manifests through various degradation pathways including photocorrosion, catalyst poisoning, and active site deactivation. Most critically, the system's inherent complexity requires simultaneous optimization of multiple components (photoelectrodes, electrolytes, and separation membranes), presenting significant challenges for industrial-scale implementation. Photocatalytic CO_2 reduction is a technology that utilizes renewable solar energy to convert CO_2 into high-value hydrocarbon fuels or chemicals. In contrast, solar energy is known as a renewable and clean energy source and is a key factor in the future transition to sustainable energy. Inspired by photosynthesis in natural biological systems, the use of artificial solar energy for producing high value-added chemicals has attracted much attention.[12] In contrast, photocatalysis uses

Guifen Li

Guifen Li is a first year PhD student at the School of Energy Materials and Chemistry, Inner Mongolia University, under the supervision of Prof. Jiangwei Zhang. She is currently focused on the synthesis of polyoxometalates and their applications in photocatalysis.

Zheyu Wei

Zheyu Wei graduated from Tsinghua University and has long been committed to the design, synthesis, structural characterization and catalytic application of polyoxometalate compounds. He has established a rational design paradigm for polyoxometalate molecular catalysts and has published more than 30 SCI papers and patents in famous journals at home and abroad. He has won the national scholarship for postgraduates and Zhongguancun U30 and other honors. At present, he is the founder and CEO of Tsing Chem Future Sky (Beijing) Nano New Material Technology Co., Ltd.

Yanru Shi

Yanru Shi received master's degree in 2013 from Inner Mongolia Agricultural University. Her current research interests focus on the theoretical study of new energy and materials processing engineering.

Ruirui Zhang

Ms Ruirui Zhang is currently enrolled at the Institute of Energy Materials Chemistry, Inner Mongolia University, where she is pursuing a master's degree under the mentorship of Professor Jiangwei Zhangi. In 2020, she graduated from the Chemistry Education program at Ningxia University, earning her bachelor's degree. Throughout her postgraduate journey, Ms Zhang has dedicated herself to the research area of electrocatalytic carbon dioxide reduction. Her primary focus lies in the design of selective catalysts for the electrochemical conversion of carbon dioxide into ethylene and ethanol.

solar energy directly to drive the reaction without the need for additional electrical or thermal energy and is a clean and renewable source of energy.[13,14] Photocatalysis is usually carried out at indoor temperature and pressure, with mild reaction conditions and low equipment requirements. Photocatalysis can significantly reduce operating costs if it can utilise solar energy efficiently. High selectivity for specific products (*e.g.*, CO, CH_4, CH_3OH, *etc.*) can be achieved by modulating the energy band structure and surface properties of the photocatalyst. Importantly, the photocatalytic process produces no secondary pollution and few by-products and is environmentally friendly.

CO_2 remains a plentiful and inexpensive carbon feedstock, despite the serious environmental problems caused by its massive emissions.[15,16] The goal of photocatalytic CO_2 reduction technology is to achieve efficient, selective, and durable conversion of CO_2 into specific products to enable large-scale utilization.[17,18] However, the activation of inert CO_2 molecules usually requires a very high energy input because the C═O bonds in CO_2 have a high bond energy. In addition, the elemental carbon in carbon dioxide can be reduced from a high oxidation state to a low oxidation state, which involves a large number of reduction products, resulting in the need for further modulation of CO_2RR selectivity. The formation and type of final reduction products depend mainly on the number of electrons and protons involved in the reaction during catalysis. In addition, the CO_2RR usually competes fiercely with the HER, which usually partially reduces the efficiency and selectivity of CO_2 conversion, resulting in a photocatalytic system whose conversion efficiency, selectivity and stability are still far from satisfactory, mainly due to the low light utilisation rate of the photocatalytic system, the limited active sites, and the fast rate of photogenerated electron–hole pair complexation.[19] To overcome these shortcomings, it is necessary to design photocatalytic systems that can adequately meet the requirements of light trapping, reactant adsorption, photogenerated charge separation and transport, and CO_2 activation.[20] Currently, POMs with well-defined and modifiable structures and good redox properties are receiving more and more attention in the field of the photocatalytic CO_2RR.[21,22] Polyoxometalates (POMs) are a large class of oxides of metals (*e.g.*, V^V, Mo^V, Nb^V, Ta^V, Mo^{VI}, and W^{VI}) representing a large number of crystalline inorganic clusters with unique physical and chemical properties.[23] POMs can be used as photocatalysts, co-catalysts, photosensitisers, and multi-electron donors in the photoreduction of CO_2.[24] Therefore, POMs and POM-based catalysts would be among the most promising catalysts for photocatalytic

Xiangyi Kong

Xiangyi Kong is a graduate student at Inner Mongolia University in Hohhot, under the supervision of Zhang Jiangwei. She is a member of the Communist Party of China and graduated from Nanjing Forestry University with a bachelor's degree. At present, her main research direction is electrocatalytic carbon dioxide reduction.

Rui Ren

Rui Ren is a second-year doctoral student at the Institute of Energy and Materials Chemistry, Inner Mongolia University, under the supervision of Zhang Jiangwei. She is currently focused on the synthesis of polyoxometalates and their applications in electrocatalysis.

Yafu Wang

Yafu Wang is an M.S. student at the Institute of Energy Materials Chemistry, Inner Mongolia University, conducting his research under the supervision of Prof. Jiangwei Zhang. He received his bachelor's degree from Ningxia University. His research focuses on the development of electrode materials for hydrogen production from seawater electrolysis and catalysts for energy materials.

Sitan Li

Dr Sitan Li is currently a postdoctoral researcher at the Institute of Energy Materials Chemistry, Inner Mongolia University. He received his PhD from the Department of Chemistry, Fudan University, in 2022. His research focuses on the synthesis and application of porous materials.

reduction of CO_2. To date, a growing number of POM structures have been found, which can be modified by altering the elemental composition, structural dimensions and thus their corresponding properties, such as redox capacity, acidity, and thermal and chemical stability. Most importantly, these POM-based compounds can often exhibit reversible multi-electron redox transitions while maintaining a stable structure.[20] To date, a growing number of POM-based compounds have been extensively explored in the photocatalytic CO_2RR, including POM clusters, POM@MOFs (encapsulation of POMs into metal–organic frameworks), POMOFs (POM-based metal–organic frameworks) and POM-g-C_3N_4 and POM-LDH, among others. They have demonstrated some outstanding strengths and important advances in these areas, but there are some serious issues that need to be solved. For example, the complex structure of POMs leads to easy decomposition, easy generation of other species on the surface, *etc.* Additionally, POMs are larger molecular clusters, which lead to their lower catalytic activity. This paper focuses on the advantages, recent advances and challenges faced by POM-based compounds as photocatalysts for the CO_2RR and proposes strategies and prospects to promote their development.

2. Basic understanding of photocatalytic carbon dioxide reduction

Excessive emission of CO_2 is the main cause of global warming, so the efficient conversion of CO_2 into valuable hydrocarbon chemicals is an effective way to solve the energy and environmental crises.[25,26] The photocatalytic reduction method as an effective strategy not only reduces the amount of CO_2 in the atmosphere, but also obtains valuable hydrocarbon products such as CO, CH_4, C_2H_4, formic acid and acetic acid.[27,28] Therefore, this catalytic method has important research value and application prospects. CO_2 is a linear molecule with a high degree of symmetry and the energy required to break the C=O bond is as high as 750 kJ mol^{-1}, which makes its structure extremely stable and resistant to chemical reactions.[29]

Thermodynamically, photocatalytic carbon dioxide reduction is a multiple electron-transfer process, and the energy required to generate different products varies.[30–32] Especially in the real reaction process, the energy required is higher than the theoretical value, and it is difficult for conventional semiconductors to meet the requirements, so it is generally believed that the activation of CO_2 is a decisive speed step.[33] Kinetically, CO_2 is a non-polar linearly symmetric molecule, where the carbon atom acts neither as an electron donor nor an electron acceptor, and the electron cloud densities of the two oxygen atoms are uniformly distributed, resulting in a stable CO_2 molecular structure and a high CO_2 activation barrier. In addition, the multi-electron reaction step slows down the carbon dioxide reduction reaction and limits the efficiency and selectivity of the CO_2 reduction reaction. Therefore, it is necessary to develop efficient photocatalysts.[34,35]

The basic process of photoreduction of CO_2 is shown in Fig. 1, in which the semiconductor acting as a photocatalyst is excited by light to generate electron–hole pairs, and the photogenerated electrons generated in the valence band (VB) subsequently jump to the conduction band (CB), while the

Yongge Wei

Professor Yongge Wei received his B.S. from Central China Normal University in 1988 and his M.S. from Wuhan University (1995). He became a faculty member of the Chemistry Department of Peking University in 1995 and was promoted to an associate professor in 1999. During 2000–2001, he was a research associate at the University of Missouri, Kansas City (USA). He joined Tsinghua University in 2005 and was promoted to a full professor in 2010. His research interests are focused on the synthesis and chemical modification of polyoxometalates and their applications in catalysis, energy and medical sciences.

Jiangwei Zhang

Prof. Dr Jiangwei Zhang is currently a "Steed plan High level Talents" Professor, "Grassland Talents", "Inner Mongolia Rejuvenation Talents" of Inner Mongolia, Principal Investigator from College of Energy Material and Chemistry under the leadership of Dean Academician Dongyuan Zhao, Inner Mongolia University. He received his PhD from the Department of Chemistry, Tsinghua University, in 2016. He has published 206 innovative publications including in Science; Nat. Catal.; JACS; Adv. Mater.; Angew.; Nat. Commun.; EES as a corresponding author with an H*-index of 55. He was recognized among the World's Top 2% Scientists in 2024. Currently, his research focuses on the common key scientific issues "materials structure and reaction mechanism dynamically and precisely visual detection and determination"; "Advanced characterization methodology and energy catalytic materials interdisciplinary"; "water electrolysis hydrogen production electrolyzing material and cell".*

holes remain in the valence band (VB).[36,37] The conduction band minimum (CBM) and valence band maximum (VBM) of the photocatalyst during the photocatalytic reaction need to include the redox potential for the CO_2 reduction reaction, and the generated photogenerated charge carriers will be able to participate in the surface redox reaction. This implies that the photocatalyst should have a conduction band potential that is more negative than the CO_2 reduction potential and a valence band potential that is more positive than the H_2O oxidation potential, with photogenerated electrons in the conduction band used for the CO_2RR and the corresponding photogenerated holes consumed either by the oxygen-extraction reaction (OER) or by an additional sacrificial electron donor for the complete catalytic CO_2RR process. Thus, the CB and VB positions of the catalyst determine the redox capacity of the catalyst in some extent.[38,39]

In addition, the separation efficiency of the photogenerated carriers has a great influence on the catalytic performance.[40] Although semiconductors can generate a large number of carriers under light conditions, some electrons may return to their original positions in the VB or complex with holes during the migration process, so that a growing number of electrons and holes arriving at the surface of the catalyst decreases, which reduces the charge separation efficiency and adversely affects the CO_2 conversion process. This low photogenerated carrier separation efficiency is a major limiting factor for the development of the CO_2RR, so minimising hole complexation or maximising carrier separation is essential for improving reduction efficiency. In conclusion, changing the band gap of semiconductor materials and enhancing the separation efficiency of photogenerated carriers of semiconductor materials are one of the important methods to enhance the catalytic performance of catalysts.[41] Therefore, an ideal CO_2RR photocatalyst should have at least the following characteristics: a good light-absorbing bandgap structure, effective separation and transport of photogenerated electron–hole pairs, and a large number of reaction sites with adsorbed activation amounts to promote the photocatalytic reaction.

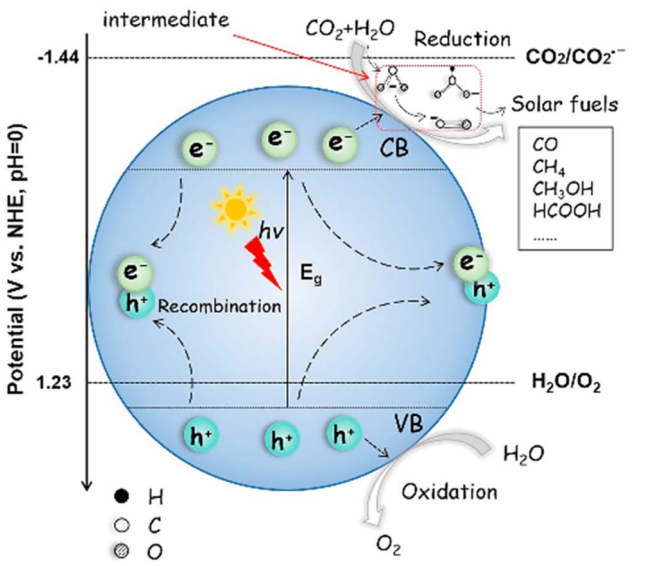

Fig. 1 Schematic diagram of photoreduction of carbon dioxide.[30]

3. Basic properties and benefits of POMs

Polyoxometalates (POMs) are a class of organotransition metal oxide cluster anions, consisting of cations and polyacid anions, in which the metal oxide octahedron is the basic constituent unit of polyacid anions, and the metals in the structure generally include pre-transition metals/transition metals (Mo, W, V, *etc.*),[42,43] which have electronic properties similar to those of metal-oxide semiconductors (MOSs) and thus have quasi-semiconducting photochemical properties. The photocatalysts have quasi-semiconductor photochemical properties.[44,45]

Common photocatalysts include zinc oxide (ZnO[46,47]), cobalt oxide (Co_3O_4 (ref. 48)), and cadmium sulfide (CdS[49,50]). Among these photocatalysts, ZnO has a high energy level valence potential and an inherent dipole structure, so ZnO has a high photogenerated carrier mobility and exhibits excellent photocatalytic activity, especially under ultraviolet light. ZnO can also be prepared in a variety of morphologies (*e.g.*, nanowires, nanorods, *etc.*) by modulating the preparation conditions, which can improve the specific surface area and catalytic performance.

However, ZnO is susceptible to photocorrosion during photocatalysis,[51] especially under acidic or alkaline conditions. ZnO mainly absorbs UV light and has low utilisation of visible light. Co_3O_4 has a narrower forbidden bandwidth (~2.1 eV) and is able to absorb visible light with higher solar light utilisation. The valence changes of Co^{2+}/Co^{3+} in Co_3O_4 contribute to catalytic reactions, particularly in redox processes. Co_3O_4 exhibits high photosensitivity in the visible spectrum but suffers from the disadvantage of low efficiency in optimal photovoltaic conversion due to the bulk effect. Although Co_3O_4 is capable of absorbing visible light, its photocatalytic efficiency is usually lower than that of materials such as TiO_2.[52] CdS has good charge separation efficiency and quantum size effect.[10] However, CdS is prone to surface defects (*e.g.*, sulphur vacancies, cadmium vacancies, *etc.*) during its preparation, which can become the centre of electron–hole complexation and promote the complexation. Moreover, CdS is prone to photocorrosion under light, resulting in the generation of Cd^{2+} and S^{2-} on the surface,[53] and these by-products will further increase the surface defect states and promote electron–hole complexation. Photocorrosion not only reduces the stability of CdS, but also increases the number of complex centres. Metal–organic frameworks (MOFs) and covalent organic frameworks (COFs) are also applied in photocatalysis.[54,55] These materials feature well-defined pore architectures and exceptionally high surface areas, providing abundant active sites for CO_2 adsorption and enabling localized reactant concentration enhancement for superior catalytic efficiency. By judicious selection of organic linkers and metal nodes, their band structures, light absorption ranges and catalytic site distributions can be precisely

engineered. However, these materials still face challenges, including hydrothermal instability (*e.g.*, Zn-MOFs degrade at pH < 5), harsh synthesis conditions (some requiring treatment at −196 °C), and high raw material costs (*e.g.*, ligands containing Pt/Pd). Mechanistic studies further require advanced operando techniques (*e.g.*, FTIR and XAS) coupled with DFT simulations. Perovskites exhibit unparalleled compositional flexibility through site engineering, enabling precise bandgap (1.2–3.0 eV) and light-harvesting optimization. Their broad spectral response (300–800 nm) surpasses conventional semiconductors, achieving superior solar utilization[56,57]. They demonstrate exceptional performance in pollutant degradation and water splitting. However, three critical issues persist: (1) environmental instability—phase segregation occurs at >60% humidity or >1 sun illumination; (2) toxicity concerns—Pb^{2+} leaching reaches 50 ppm in lead-based variants; (3) activity decay—40% efficiency loss after 100 h operation.

Compared with these common photocatalysts, POMs have significant advantages. POMs have excellent thermal stability, high activity, and good ability to carry and release electrons and can achieve rapid electron transfer without changing the structure, thus improving the photocatalytic efficiency. They demonstrate great advantages in catalysis.[58,59] In addition, the fully inorganic nature and robust shell topology make POMs attractive homogeneous photocatalysts.[60] The tunable redox potential and reversible redox activity are the main advantages of polyoxometalates as photocatalysts.[34] However, conventional POM structures tend to have a large light-absorbing bandgap in the UV region, which limits the photocatalytic efficiency. So, it can be modulated by the following strategies. Firstly, photosensitisers that respond to visible light can be added. For example, ruthenium pyridine and noble metal-free metalloporphyrins were added to the catalytic system to help modulate the light absorption range of POMs.[61,62] Because POMs have strong electron acceptability, which enables them to effectively accept photoexcited electrons transferred from the LUMO energy level of the photosensitiser, when the LUMO energy level of the photosensitiser is more negative than that of POMs, the POMs can act as electron reservoirs to spontaneously accept electrons from the photosensitiser. The electrons in the photosensitiser can be rapidly transferred to the POM catalyst by continuous photoexcitation, so that the polymetallic oxonate can promote the transfer of photogenerated carriers and prolong the lifetimes of the photogenerated carriers in the photosensitiser to inhibit the complexation of electron–hole pairs, which significantly improves the photocatalytic efficiency of the photocatalytic carbon dioxide reduction.

Secondly, the structure of different valence states of POMs (namely, heteropoly blues, denoted as HPBs) can be modulated, thereby changing the energy band structure and light absorption range.[63] The absorption spectra of some heteropoly blues may have rather broad light absorption covering the visible or near-infrared region, which will greatly improve the utilisation of sunlight and thus the photocatalytic efficiency of photocatalytic carbon dioxide reduction. Furthermore, polyoxometalates in the reduced state are better able to enrich electrons relative to their oxidised state, which then changes their LUMO and HOMO energy levels. Thus, when metallic or even non-metallic elements with different electronegativities are introduced into the POM structure, their LUMO energy levels may change. This can be used to tune the electronic or surface structure of POM-based composite photocatalysts to improve the photocatalytic CO_2 reduction performance.

3.1 Structure and synthesis of POMs

Polyoxometalates are a class of anionic clusters formed from transition metal ions (*e.g.*, tungsten, molybdenum, vanadium, *etc.*) and oxygen atoms connected by shared apex oxygen atoms.[64] They are classified into homopolyacids and heteropolyacids according to the presence or absence of heteroatoms. Polyacids without heteroatoms are homopolyacids (*e.g.*, $[Mo_6O_{19}]^{2-}$, $[Nb_6O_{19}]^{8-}$, $[W_6O_{19}]^{2-}$, and $[Ta_6O_{19}]^{8-}$). Polyacids containing heteroatoms are heteropolyacids, which can be classified into six typical configurations based on the geometrical configuration of the heteroatoms and the ratio of heteroatoms to ligand atoms: the Keggin, Dawson, Anderson[65], Waugh[66], Silverton[67] and Lindqvist[68] structures. Each structure type has a unique geometry and charge distribution. These structural properties enable POMs to exhibit unique catalytic performance in photocatalytic carbon dioxide reduction. Some generalisations regarding the synthesis of polyoxometalates with the classical six structures are given below:

(1) Keggin structure. It is usually prepared by acidifying an acid salt solution containing tungsten or molybdenum and adding an appropriate reducing agent (*e.g.* phosphoric acid, sulphuric acid, *etc.*).[69] For example, tungsten phosphates with the Keggin structure can be obtained by acidifying sodium tungstate solution with phosphoric acid, followed by heating, crystallisation, *etc.* The Keggin structure is characterised by the fact that heteroatoms with tetrahedral configuration (*e.g.* P, Si, *etc.*) are located in the centre, surrounded by 12 metal–oxygen octahedra. There are two classical methods for the specific synthesis of $H_3[\alpha\text{-}PW_{12}O_{40}]$ as an example.

Method 1: sodium tungstate is dissolved in water, heated to boiling until the solution clarifies, and phosphoric acid is added. Concentrated hydrochloric acid is then added slowly and cooled to obtain a crystalline product but it contains a small amount of tungstic acid. After 4 h, the product is re-dissolved in water after filtration under reduced pressure and extracted with ether and concentrated hydrochloric acid. The bottom polyacid ether complex was then added to the water, ether and hydrochloric acid solution and extracted again, and the bottom layer was an ether complex of the colourless thick liquid $H_3[PW_{12}O_{40}]$. The ether complex was then added to water and the water bath was heated until the bottom solution gradually disappeared and $H_3[\alpha\text{-}PW_{12}O_{40}]$ crystals were produced.

Method 2: sodium tungstate and disodium hydrogen phosphate are dissolved in boiling water. Concentrated hydrochloric acid solution is added drop by drop under stirring, and when the solution is cooled, anhydrous ether is added for extraction, followed by washing with water several times. Finally, the ether compounds are collected and subjected to heat evaporation in a water bath to obtain the crystalline product.

(2) **Dawson structure.** The synthesis is similar to the Keggin structure, but usually requires more complex reaction conditions and longer reaction times. The structure of the product can be optimised by adjusting the ratio of reactants, reaction temperature time and temperature.

The Dawson structure is characterised by two Keggin structural units joined by sharing an oxygen atom to form a dimer structure. Taking $K_6[\alpha\text{-}P_2W_{18}O_{62}]$ and $K_6[\beta\text{-}P_2W_{18}O_{62}]$ as examples, there are various synthetic methods, which need to be used in controlling the reaction temperature, the reaction time and the temperature of the recrystallisation solution. We mainly introduce the synthesis method with the highest yield and the least by-products reported so far. The specific synthesis steps were as follows: sodium tungstate was slowly added into water with vigorous stirring, and 4 mol per L hydrochloric acid solution was dripped into the aqueous solution of sodium tungstate with a dropping funnel, and the pH of the reaction mixture changed to 6–7 after the hydrochloric acid solution was added, and the pH of the reaction mixture became 6–7 when the dilute solution was clarified, and then immediately 4 mol per L phosphoric acid solution was added dropwise to the reaction mixture, and after the addition of phosphoric acid, the solution became a yellowish clarified solution, and the pH became 1–2. The solution was refluxed for 24 h, then added to the reaction mixture containing 4 mol L^{-1} phosphoric acid. After subsequent refluxing for another 24 h, the solution turned bright yellow.[2] The solution was transferred to a wide-mouth bottle, cooled to room temperature and left for 3–4 h, during which the yellow colour faded. KCl was added at room temperature with stirring, resulting in a yellow precipitate, which was filtered and dried in air to obtain the crude product. The crude product was dissolved in water and heated to 80 °C. After heating for 72 hours, small yellow crystals formed at the bottom of the bottle. The advantage of this method is the high purity and good crystallinity of the product, which is widely used in laboratory studies.[70,71]

(3) **Anderson structure.** The Anderson structure is an octahedral configuration with six metal–oxygen octahedra around a central heteroatom (usually Al, Fe, *etc.*). The synthesis step for the Anderson structure is mainly the conventional synthesis method: metal salts, ligands and solvents are mixed in a certain ratio. The mixture is heated to boiling and refluxed for a period of time to ensure complete reaction of the reactants. At the end of the reaction, the solution is cooled to indoor temperature and the crystal product is obtained by filtration or centrifugation. The crystal product is recrystallised or otherwise purified as required.[72] The method has relatively mild synthetic conditions.

(4) **Waugh structure.** The synthesis of the Waugh structure usually involves a multi-step reaction including dissolution of the metal salt, addition of ligand, pH adjustment and subsequent crystallisation process. The Waugh structure is characterised by two triple-deficient Keggin structural units connected by sharing three oxygen atoms to form a cluster. The synthesis steps of the Waugh structure: molybdenum and manganese ligands were used as raw materials and prepared using an ethanol–water mixed solvent system. The molybdenum ligand and manganese ligand were placed in a beaker and a mixed solvent of ethanol and water was added. The mixture was thoroughly stirred, and the pH was adjusted. Ammonium persulfate (APS) was then added as a hydrolyzing agent. The temperature was raised, and the mixture was stirred for 30 min. After cooling to room temperature, the product was filtered, washed, and dried to obtain molybdenum–manganese heteropolyoxometalate powders with the Waugh structure. For example, the synthesis of $H_6[MnMo_9O_{32}]$ requires only the addition of manganese sulfate and ammonium persulfate to a 10% excess $(NH_4)_6Mo_7O_{24}$ solution at 95 °C. The mixture is reacted under reflux for 5 min, then rapidly cooled, filtered, and recrystallized in hot water at 70 °C to obtain orange crystals.[73] If it is desired to prepare polymetallic oxalates with a Waugh structure containing other metal cations, they can be prepared by an ion exchange method after the synthesis of $H_6[MnMo_9O_{32}]$.

(5) **Silverton structure.** The Silverton structure has a special cage-like structure in which metal–oxygen octahedra are arranged and connected in a specific way. The synthesis of this structure is usually complex and requires precise control of the reaction conditions and the ratio of reactants. Taking the synthesis of $(NH_4)_6[H_2CeMo_{12}O_{42}]\cdot 9H_2O$ as an example, there are two main synthetic methods.

Method 1: 5% cerium ammonium nitrate solution was added to 0.25 mol per L boiling $(NH_4)_6Mo_7O_{24}\cdot 4H_2O$ solution, dilute sulfuric acid was added dropwise to make the solution saturated at 65 °C. After cooling, saturated ammonium nitrate solution was added, followed by evaporation and crystallisation to obtain light yellow crystals; the product obtained by filtration was washed several times with methanol, dissolved in hot water to crystallise, and then washed with methanol to obtain the product, which was obtained through the ion exchange method and can be converted ammonium salts to heteropolyacids.[74]

Method 2: $(NH_4)_6Mo_7O_{24}\cdot 4H_2O$ was dissolved in water and heated until fully dissolved and then cerium sulphate was added into the solution and boiled for 15 min, and cooled to room temperature. Ammonium nitrate was then added, and the precipitate was filtered, washed with saturated ammonium nitrate solution, and then washed twice with methanol solution to obtain the crude product. The crude product was dissolved in 0.2 mol per L sulphuric acid solution to obtain a yellow clarified solution, which was immediately filtered into a mixture of ammonium nitrate and water without stirring, and crystals were slowly precipitated at the interface of the two solutions.[75]

(6) **Lindqvist structure.** The Lindqvist structure is a homopolyacid structure formed by six metal atoms connected by oxygen atoms in the absence of heteroatoms. The synthesis of Lindqvist structure POMs with $W_6O_{19}^{2-}$ as an example mainly includes the following steps: sodium dehydrated tungstate is dissolved in acetic anhydride and dimethylformamide. The solution is heated to 100 °C for two and a half hours and a mixture of acetic anhydride, hydrochloric acid and DMF is added. Filtration was carried out and the filtrate was collected and stirred. Tetrabutyl ammonium bromide was dissolved in methanol and added to the stirred filtrate, which was then

washed three times with methanol. Finally, the collected white powder was dissolved in a very small amount of hot dimethyl sulfoxide and left overnight in a refrigerator at −20 °C to obtain colourless rhombic crystals.[76]

In summary, in terms of synthesis conditions, Keggin-type polyoxometalates demonstrate the most facile formation conditions. Waugh and Silverton architectures necessitate either stringent templating agents or significantly elevated reaction temperatures. Lindqvist-type clusters require strongly alkaline media for successful synthesis. Anderson structure formation exhibits pronounced dependence on the identity of the central heteroatom. In terms of structural characteristics, Dawson and Silverton clusters are characterized by their considerable molecular dimensions. Waugh polyoxometalates possess unique three-dimensional topological configurations. Both Keggin and Lindqvist structures exhibit exceptionally high symmetry elements. In terms of stability and modulation considerations, Keggin isomers demonstrate remarkable structural controllability during isomerization processes. Waugh-type compounds show inherent thermodynamic instability and decomposition tendencies. Silverton architectures require stabilization *via* coordination with rare-earth metal cations (S1).

4. POM-based materials in the photocatalytic CO_2RR

4.1 Metal-modified and morphology-modified POM materials

As molecular photocatalysts with semiconductor photochemistry,[77] polyoxometalates (POMs) also offer many advantages in CO_2 photocatalytic reactions, such as excellent solubility, heat stability[78] and tunable redox activity.[79] POMs have good solution stability that enables them to photocatalyse the CO_2RR in water or other solvents and to assist in the reduction of CO_2 to other products.[80] In order to optimise the performance of POMs in photocatalytic CO_2 reduction, the structure of POMs needs to be modulated. By changing the composition and structure of POMs, their light absorption, redox capacity and electron transfer capacity can be regulated.[81] The light absorption of POM photocatalysts in the ultraviolet region can be extended by introducing different transition metal ions or ligands to extend the light absorption range of POMs, which enables the use of a wider range of sunlight for photocatalytic reactions. Such POM-based photocatalysts modified with transition metals require the addition of auxiliary noble metal photosensitisers to the reaction system, and the catalytically active sites are usually the introduced transition metal ions rather than ions in the POM structure itself.

In 2010, Neumann and coworkers first synthesised $\{(C_6H_{13})_4N\}_5[Ru(H_2O)SiW_{11}O_{39}]$, a structure of Keggin POMs substituted by Ru, which can reduce CO_2 to CO under light conditions.[82] Experimental results showed that the Ru site plays an important role in CO_2 activation, whereas the POMs ($[SiW_{11}O_{39}]^{8-}$) act as photocatalysts in the photocatalytic process.

In addition, Zhang's team discovered a polymetallic oxalate photocatalyst ($[Mn(en)_2]_6[V_{12}B_{18}O_{54}(OH)_6]\cdot 17H_2O$) (abbreviated as Mn_6V_{12}).[83] This metal Mn-modified polymetallic oxalate catalyst generates CO with a selectivity of 90.3% and H_2 with a selectivity of 9.7%. According to the experimental results, the energy levels of Mn_6V_{12} at the highest occupied molecular orbital (HOMO) and the lowest unoccupied molecular orbital (LUMO) are 0.99 eV and −0.77 eV, respectively. The highest occupied molecular orbital (HOMO) and the lowest unoccupied molecular orbital (LUMO) of $[Ru(bpy)_3]Cl_2$ are 1.24 eV and −1.25 eV, respectively. Thanks to the LUMO energy level of $[Ru(bpy)_3]Cl_2$ being more negative than that of Mn_6V_{12}, the electrons on $[Ru(bpy)_3]Cl_2$ are preferentially transferred to Mn_6V_{12}. In the reaction process, the main role of the photosensitizer is to absorb light and generate a large number of photoelectrons after being excited by light, and the transition metal in POMs is the CO_2 reduction centre in the system, and the photoelectrons generated by the photosensitizer by light excitation are transferred to the metal ions on the framework of the POMs, and CO_2 reduction is carried out afterwards.

Applying POMs in photocatalytic CO_2 reduction, the above research cases also require precious metals or photosensitizers for assisted catalysis, so it is more necessary to design photocatalysts that are feasible and green and only have POMs as the catalytic system in order to meet the principles of green environmental protection and energy saving.

In 2018, Barman *et al.* reported a reductive POM-based catalyst ({Mo16}) that simply regulates the central oxidation state of the metal in the POMs, with an ε-Keggin structure (Fig. 2a) terminated by (MoO_3), so that water itself acts as a solvent and sacrificial agent and selectively converts CO_2 to HCHO[84] in the absence of a photosensitizer. The transformation path and possible mechanism are shown in Fig. 2b and c. Under light irradiation, {Mo16} enters the excited state after being excited by light and produces a large number of photogenerated electron–hole pairs. The further storage of electrons and protons on the POMs enhanced the reduction ability of the POM clusters, and then CO_2 was reduced to HCHO and HCOOH by the stored electrons and protons on the POMs, while the generated holes oxidised the water to form O_2. The whole process was green and energy-saving, which provided a simple and convenient way for the design of POMs for the application of photocatalytic CO_2 reduction. The whole catalytic process is green and energy-saving, which provides a simple and convenient path for the design of POM materials for photocatalytic CO_2 reduction.

Furthermore, in addition to modifying polyoxometalates with metal ions, it is also possible to morphologically tune POM materials to have more active sites, a strategy that has also attracted much attention in photocatalytic carbon dioxide reduction. Ding *et al.* used a simple hydrothermal etching and annealing method to tune the morphological evolution of dodecahedral $K_3PW_{12}O_{40}$ (ref. 83) (Fig. 3). Some catalysts with yolk–shell and hollow structures were successfully prepared, and the yolk–shell or hollow structures would efficiently trap CO_2 while exposing more active sites. The photocatalytic activity was enhanced by using polyoxometalates with variable

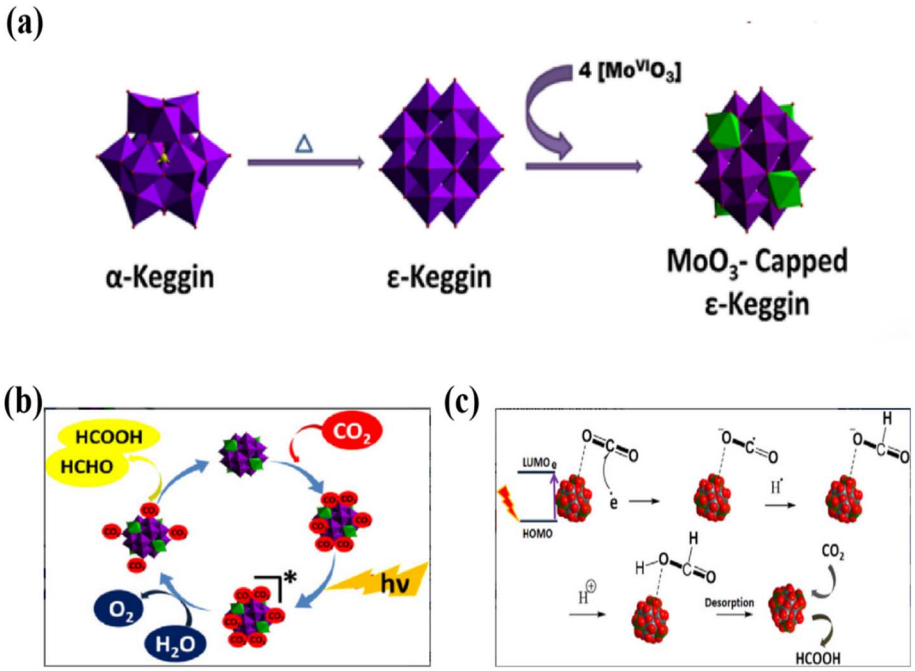

Fig. 2 (a) Possible formation pathway of the {Mo16} unit; (b) proposed plausible mechanism for CO_2 photoreduction; (c) schematic diagram showing a proposed mechanism for the reduction of CO_2 to formic acid.[84]

morphology as carriers and incorporating Co and CoNi as catalytically active sites. It was successfully used for photocatalytic carbon dioxide reduction, which significantly improved the selectivity of the product CO and provided a new idea for the design of efficient and morphology-modulated photocatalysts for POMs.

4.2 POMOF

Polyoxometalate-based Metal–Organic Frameworks (POMOFs) are a new class of hybrid materials combining polyoxometalates with Metal–Organic Frameworks (MOFs). These materials combine the advantages of POMs and MOFs with unique structural and functional properties and are widely used in the fields of catalysis,[85] electrochemistry[86] and photochemistry.[87] Polyacid-organometallic framework materials (POMOFs) are obtained by a self-assembly strategy by connecting functional POMs with linkers and introducing them into the pores of MOFs in the form of template units.[88,89] They can remain stable in aqueous solution.[43] The combination of the two facilitates structural stability and functional diversity, giving full play to their respective advantages, thereby generating the unique functionality of POMOF composites.

For example, Lan's team reported a novel stable two-dimensional sandwich planar structure POMOF (NNU-29) photocatalyst, where the introduction of strongly reducing POM units ($\{Zn_4PMo_8{}^{V}Mo_4{}^{VI}\}$) into the NNU-29 structure (Fig. 4a–d) enabled NNU-29 to efficiently convert CO_2 into HCOOH[90] (Fig. 4e). Due to the introduction of hydrophobic ligands, NNU-29 has high chemical stability. Meanwhile, the hydrophobicity inhibited the precipitation of hydrogen to a certain extent. ε-$\{Zn_4PMo_{12}O_{40}\}$ is a cluster with excellent reducing properties, which prompted NNU-29 to exhibit excellent multiphase catalytic performance for CO_2 photoreduction. The relationship between the structure of POMs and the properties of NNU-29 is exploited through a rational synthetic strategy to design the structure of a stable functional ligand with reducing properties (POMOFs), which will have an important impact on the activity and selectivity of POMs in enhancing CO_2 photoreduction.

In 2023, Su's team successfully prepared two new POMOFs based on ($[W_{10}O_{32}]^{4-}$) named compound **1** and compound **2**.[91] In the catalytic system with a photosensitiser, water, triethanolamine and acetonitrile under a pure CO_2 atmosphere, syngas was the main product, and the yield of compound **1** was 40% higher than that of compound **2** (Fig. 5a and b). Moreover, the yield of compound **1** reached 42.7 μmol h^{-1} when the CO_2 concentration was 15%, which indicated that this POMOF catalyst could not only overcome the low CO_2 concentration, but also tolerate the harsh gas compositions in the flue gas. The energy level structures and charge transfer machines of compounds **1** and **2** were inferred by Mott–Schottky. Compound **1** has a CB value of 0.82 V and compound **2** has a CB value of 0.75 V (*vs.* NHE) (Fig. 5c and d). The valence bands (VB) of compounds **1** and **2** are 1.91 V and 2.16 V (*vs.* NHE). The energy level structures of compounds **1** and **2** suggest that they can both be used for syngas preparation ($CO_2/CO = 0.53$ *vs.* NHE; $H^+/H_2 = 0.42$ *vs.* NHE). The difference in the catalytic effect may be due to a larger difference in energy levels between compound **1** and the reduction product, which may be more favourable for the reduction reaction. Density-functional theory (DFT) calculations showed that the charge distribution and spatial site resistance of compound **1** favored the reduction reaction. The

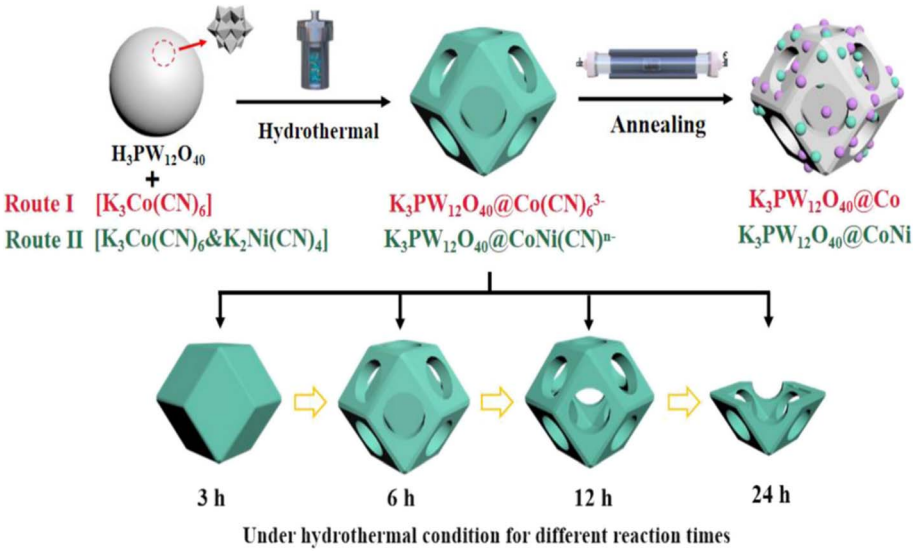

Fig. 3 Schematic illustration of the formation of the hydrothermal intermediate product $K_3PW_{12}@Co(CN)_6^{3-}$/$K_3PW_{12}@CoNi(CN)^{n-}$ and the annealed product $K_3PW_{12}@Co$/$K_3PW_{12}@CoNi$.[83]

application of POMOFs to the production of syngas products is still in its infancy, and this work provides new insights into the application of POMOFs to the photocatalytic preparation of other products.

4.3 Composite of POMs with carriers (POM@MOF)

Compounding POMs with carriers can improve their stability and reusability.[92,93] Commonly used carriers include inorganic materials such as silica,[94] alumina,[95] zeolites[96] and organic materials such as polymers and MOFs.[97] These carriers have good pore structures and surface areas, which can provide more active sites and promote the photocatalytic reaction. At the same time, the carriers can also protect the POMs from external environment damage and improve their stability and reusability.[98] Among them, MOFs, as an attractive class of organic–inorganic porous materials, consist of inorganic secondary structural units (metal oxide clusters or metal ions) coordinated with organic portions.[99,100] They have unique advantages over conventional inorganic materials, such as high porosity, good thermal stability, and good properties such as designable structures, and have demonstrated excellent performance in the field of catalysis.[101–103] In addition to this, they are also a class of highly crystalline solid materials with significant advantages such as thermal stability and recyclability.[93,104] Due to the atomic-level crystal structure and high surface area of MOFs, a growing number of catalytically active sites can be introduced into MOFs, which in turn provide excellent activity and selectivity. The coordinating unsaturated metals of MOFs can be used as single-point catalytic reaction centres for redox reactions. The ligand-unsaturated metals of MOFs can also be used as single-point catalytic reaction centres for redox reactions or as binding sites for anchoring catalytically active sites.[105]

Caroline Mellot-Draznieks' team encapsulated a POM in the cavity of a MOF by *in situ* synthesis and then introduced a Rh catalytic complex *via* post-synthesis joint exchange.[106] The Keggin-type POM ($PW_{12}O_{40}^{3-}$) and the catalytic complex Cp*Rh(bpydc)Cl_2 catalyst were co-immobilised on the Zr(IV)-based metal–organic skeleton UiO-67 to synthesise a new composite (PW_{12}, Cp*Rh)@UiO-67 (Fig. 6).

The reduction of CO_2 to formate and the production of H_2 were significantly enhanced when compared to the POM-free Cp*Rh@UiO-67 material, while Cp* Rh-free PW_{12}@UiO-67 showed no catalytic activity. A combination of density functional theory (DFT) calculations and pair distribution function (PDF) analysis using laboratory X-rays was used to characterise the POM@MOF composites and clearly demonstrate the integrity of the POM before and after catalysis. In addition, the two environments of the POM within the MOF cavities identified by DFT calculations and solid-state NMR, as well as the effect of the POM on the electronic structure of the Rh catalytic center, enable the study of POM-based composites of MOFs and provide a new strategy for improving photocatalytic performance.

In POM@MOF, cluster-based MOFs have a unique long-range ordered spatial structure with regular intrinsic pores that enable monodispersion of POM at the molecular level.[107,108] Uniformly dispersed and well-defined metals in the MOF backbone can act as catalytically active sites. However, only a few homogeneous POM-based molecular catalysts have been reported to study the role of electron transfer processes in the photocatalytic CO_2 reduction reaction.[109] Because non-homogeneous photocatalysts contain a variety of components, they often exhibit unclear compositions, unclear atomic structures, and complex dynamic transitions of the active centers, making it difficult to fully understand the electron transfer pathways as well as photocatalytic mechanisms.[110]

To solve this problem, Li *et al.* synthesised a series of novel Keggin-type POM-coated cadmium atom clusters of organo-skeletal crystalline materials (POM@CdMOF) as a photocatalyst

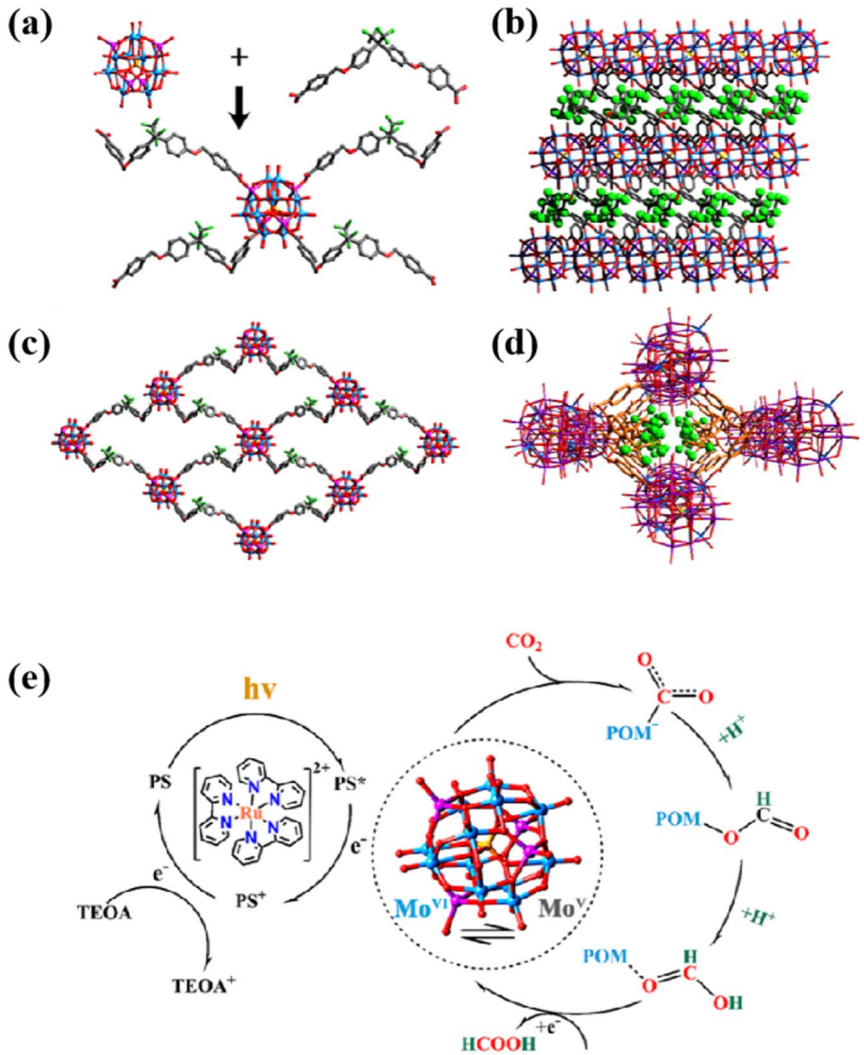

Fig. 4 (a) NNU-29's coordinated environment; (b) 2D single-layer network; (c) POM layers and trifluoromethyl layers forming a sandwich-like structure along the *b*-axis. (d) A rhombic channel full of trifluoromethyl along the *c*-axis. (e) Mechanism of CO_2 reduction of HCOOH by NNU-29.[90]

model. POM@CdMOF has a well-defined crystal structure, and systematic studies were conducted to elucidate, at the molecular level, the different electron transfers in the process of reactant adsorption and conversion in multiphase photocatalysis.[111]

Combined *in situ* transient photovoltage (TPV) measurements and femtosecond transient absorption (TA) spectroscopy studies (Fig. 7a and b) demonstrate that in POM@CdMOF systems, different polyoxometalate (POM) guests exhibit distinct electron storage and transfer capabilities. These differences lead to varied electron transfer pathways between POM and CdMOF components, consequently inducing different charge separation behaviors (Fig. 7c and d). Multiphase catalysis is significantly affected. Moreover, the electron transfer behavior during POM@CdMOF photocatalysis also affects the adsorption behavior of CO_2 molecules, which regulates the adsorption free energies of different reactions in the intermediates and consequently affects the product selectivity, as revealed by density functional theory (DFT) calculation (Fig. 7e and f). This work provides a molecularly accurate structural model for revealing the electron transfer mechanism of the multi-field multiphase photocatalytic CO_2RR reaction as well as a clearer and more intuitive understanding of the process of electron transfer inside the MOF-coated POM photocatalyst at the molecular level.

4.4 POM-g-C_3N_4

Most inorganic semiconductors have large bandgap widths and therefore only exhibit strong catalytic activity in the ultraviolet region. Because of their inherent non-porous structure, photocatalytic reactions can only be carried out on the outer surface of the catalyst, which means that a large number of photogenerated electron–hole pairs will be complexed within the catalyst body. Therefore, in recent years, a novel two-dimensional layered organic semiconductor, graphitic carbon nitride (g-C_3N_4),[112] has come to the attention of scientists due to

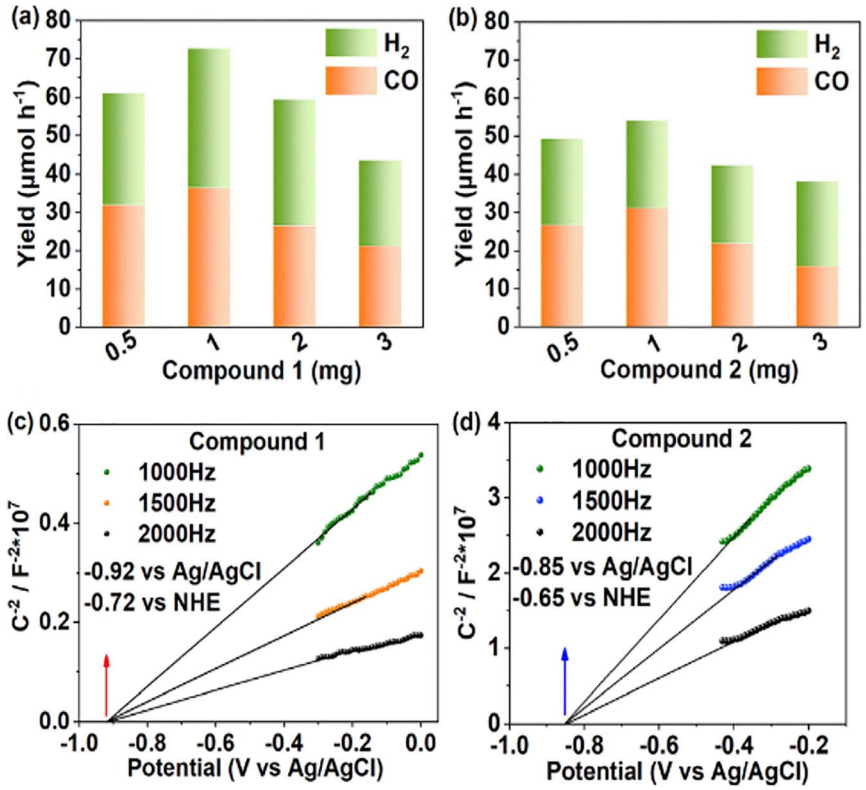

Fig. 5 (a) and (b) Products of adding different masses of catalysts for compounds **1** and **2**; (c) and (d) Mott–Schottky plots for compound **1** and **2** at frequencies of 1000, 1500 and 2000 Hz.[91]

its attractive electronic structure and easy accessibility, as well as good thermal and chemical stability.[113,114] Unlike conventional semiconductors, which are active only in the ultraviolet region, g-C_3N_4 is a visible-light active photocatalyst.[115,116] Its unique C and N atoms are sp^2 hybridised to build a highly exotic π-conjugated system, a structural feature that confers excellent visible-light responsiveness and semiconductor properties. In addition, it is crucial to extend their lifetimes and avoid electron–hole pair complexation to improve the photocatalytic efficiency.[117] In order to improve the electron transfer capacity of POM-based catalysts, the electron transfer pathway can be optimised by modulating the structure of the POMs and the complexation mode with other catalysts. Semiconductor heterojunctions facilitate fast charge separation and thus become an important strategy for efficient solar energy conversion. Compared with conventional heterojunctions, ultrathin layered

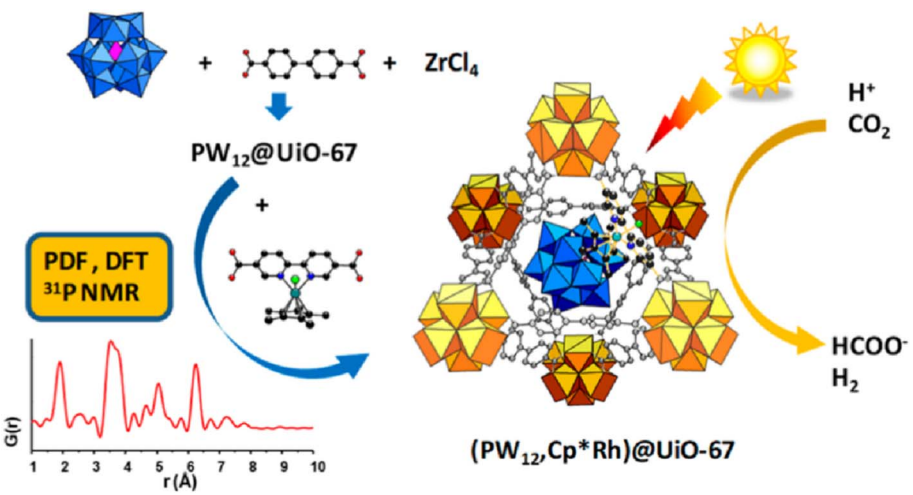

Fig. 6 Schematic diagram of the synthetic route and photocatalytic structure of the Cp*Rh@UiO-67 material.[106]

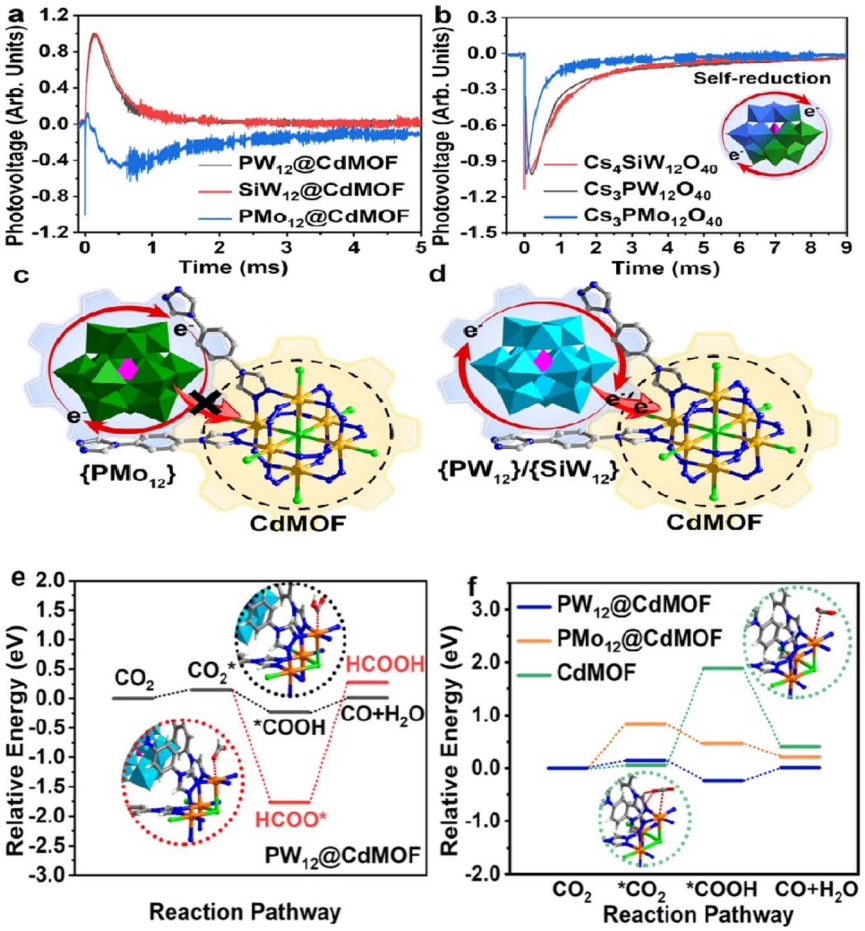

Fig. 7 (a) and (b) TPV curves of POM@CdMOF and cesium salt of parent POMs. (c) Graph of the $\{PMo_{12}\}$ cluster in PMo_{12}@CdMOF. (d) Graph of the electron transfer pathway between the $\{PW_{12}\}/\{SiW_{12}\}$ cluster and CdMOF. (e) Calculated relative energy diagrams for CO_2 reduction to CO or HCOOH. (f) DFT calculations of CO_2 reduction to CO were conducted on the optimized POM@CdMOF and CdMOF.

heterojunctions have attracted much attention due to their strong chemical bonding between monolayers, which greatly enhances the charge separation.

Sun *et al.* successfully prepared a low-cost and highly efficient composite catalyst (Co_4@g-C_3N_4) with a staggered energy band arrangement by introducing Co_4, an oxidised polymetallic oxonate free of noble metals with oxidising ability, into the semiconducting material g-C_3N_4 for the first time (Fig. 8a shows the schematic diagram of the photoinduced electron–hole pair transfer process).[118] The Co_4@g-C_3N_4 composite exhibits a high yield as well as excellent selectivity (Fig. 8b). Experimental and test results indicate that the introduction of Co_4 can improve the catalytic oxidation ability of the catalyst's surface, which is favourable for the CO_2RR on g-C_3N_4. Therefore, it is of great significance to select suitable strategies to creatively combine g-C_3N_4 with oxidised polyoxometalates, to change the original energy band structure, and to purposefully design POM-based materials to meet the requirements of being used as a photocatalyst for CO_2 reduction, which is important for improving the activity and selectivity of CO_2 photoreduction.

Wei *et al.* successfully modified saturated and vacant PW_x on g-C_3N_4 nanosheets *via* electrostatic interactions for photocatalytic CO_2 reduction.[119] Both g-C_3N_4 and POM alone produced few CO products, but the introduction of a vacant POM could significantly steer the reaction pathway and efficiently achieve the highly selective conversion of CO_2 to CH_4 by constructing a tandem system. In the catalytic process, CO_2 is first activated on g-C_3N_4 to form *CO intermediates (Fig. 9a–d), while photogenerated electrons generated by g-C_3N_4 are transferred to PW_x. The reduced PW_x then captures *CO and subsequently hydrogenates the intermediates to CH_4 (Fig. 9e). Both experimental characterisation and theoretical calculations show that in this system, g-C_3N_4 can act as a catalytic center to effectively activate CO_2 to *CO, and the resulting generated *CO intermediate can be stabilised and reduced on PW_9 by forming a π-bond with W on $[PW_9]^{2-}$. This study offers a new idea for the application of materials with g-C_3N_4 modified deficient POMs in the photocatalytic CO_2RR (Fig. 9f).

4.5 POM-LDH

Layered double hydroxides (LDHs) are a class of anionic multifunctional materials with layered structures, which have the advantages of simple synthesis, diverse compositions, and adjustable chemical compositions of the layered structures for

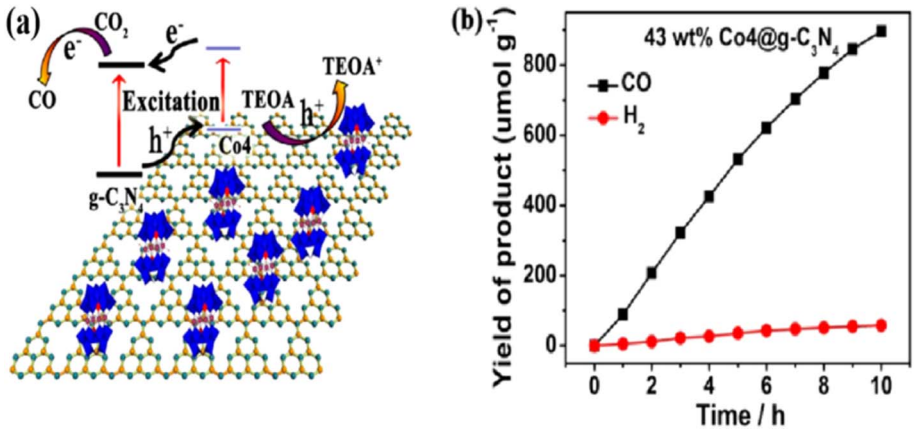

Fig. 8 (a) Schematic diagram of the photoinduced electron–hole pair transfer process; (b) yield of H_2 and CO of CO_2.[118]

various catalytic reactions.[120,121] Due to their favourable energy band positions, much attention has been directed to their application in photocatalytic CO_2 reduction.[122] In recent years, polymetallic oxonate intercalated layered double hydroxide (abbreviated as POM-LDH) nanocomposites have attracted much attention in the field of catalysis. Such composites not only inherit the intrinsic properties of POMs and LDHs, but also exert remarkable synergistic effects in the catalytic process.[123] The anionic POM is negatively charged and can be embedded in the LDH interlayer, and it can modulate the electronic structure of the metal active center of the LDH laminate, which leads to the optimization of the performance of photocatalytic CO_2 reduction. Introducing POM anions into the interlayer channels is a simple and effective method to immobilise the POM. The combination of POM-supported LDH offers several advantages, including an extended interlayer channel height, controlled loss of POM components in polar solvents, improved specific surface area of the LDH and POM, and ease of isolation and recycling from the reaction.[124]

Song *et al.* prepared NiAl–Mo_7O_{24}, a photocatalyst with hydroxyl vacancies and a suitable Ni active center, by inserting polymetallic oxonate ions into a NiAl-LDH interlayer by ion exchange.[125] The energy band structure of the modified photocatalyst, NiAl–Mo_7O_{24}, was altered to better accept electrons from photosensitizers, which facilitated the photocatalytic process of photogenerated carrier separation and transfer, which contributes to the efficient reduction of CO_2. Experimental and theoretical calculations (Fig. 10a and b) reveal that the presence of hydroxyl vacancies and the filling of interlayer ions together improve the electronic structure of the lamellar metal active center. The adsorption of CO and its subsequent hydrogenation reaction are facilitated on the Ni sites with an electron-rich environment, and the energy barrier of the coupling reaction of CO_2 hydrogenation to produce OCOH (Fig. 10c and d) and CH_3 intermediates is reduced. Thus, the efficient and rapid conversion of CO_2 to C_2H_6 was promoted (Fig. 10e and f). The yield of C_2H_6 *via* the CO_2RR under visible light was 246.70 μmol g^{-1} h^{-1}. This article provides a new strategy for photocatalytic production of C2 products through the synergistic effect of POMs and LDH and provides valuable insights into the formation mechanism of C2 chemicals at the atomic level.

POM-LDH nanocomposites have been synthesised by a variety of methods,[126] such as an *in situ* synthesis method[127] and a hydrothermal method.[128] The main ones include the primary layer modification method[129] and the exfoliation assembly method.[130,131] The primary layer modification method prepares intercalated POM-LDH nanocomposites by chemically modifying the surface of LDH laminates, *e.g.*, by introducing functional groups (*e.g.*, carboxyl groups, amino groups, *etc.*) or by surfactant modification, so that they can have specific interactions with the POM. This method is not only simple to perform, but also can effectively control the structure and properties of the composites. The peel assembly method involves peeling the LDH lamellar structure into single or a few layers of nanosheets, which are then reassembled with POM anionic clusters into composites by electrostatic interaction or covalent bonding links. This method is able to prepare POM-LDH nanocomposites with a higher specific surface area and abundant active sites, and at the same time, it can achieve the precise assembly of the POM and LDH.

POM-LDH nanocomposites have extensive applications in catalysis, covering electrocatalysis, photocatalysis, thermocatalysis and so on. In the field of photocatalysis, POM-LDH nanocomposites have also been used in photocatalytic degradation of organics,[132] photocatalytic hydrogen production and other reactions, showing good catalytic performance.[133] In conclusion, POM-LDH nanocomposites, as an emerging multifunctional nanocomposite, show a broad application prospect in the field of catalysis.

5. Challenges and future perspectives

Although POMs show great potential for application in photocatalytic CO_2 reduction, they still face some challenges. Firstly, most POMs only absorb in the ultraviolet region, which limits their utilisation of sunlight. Expanding their light absorption range to the visible or even near-infrared light region is an urgent

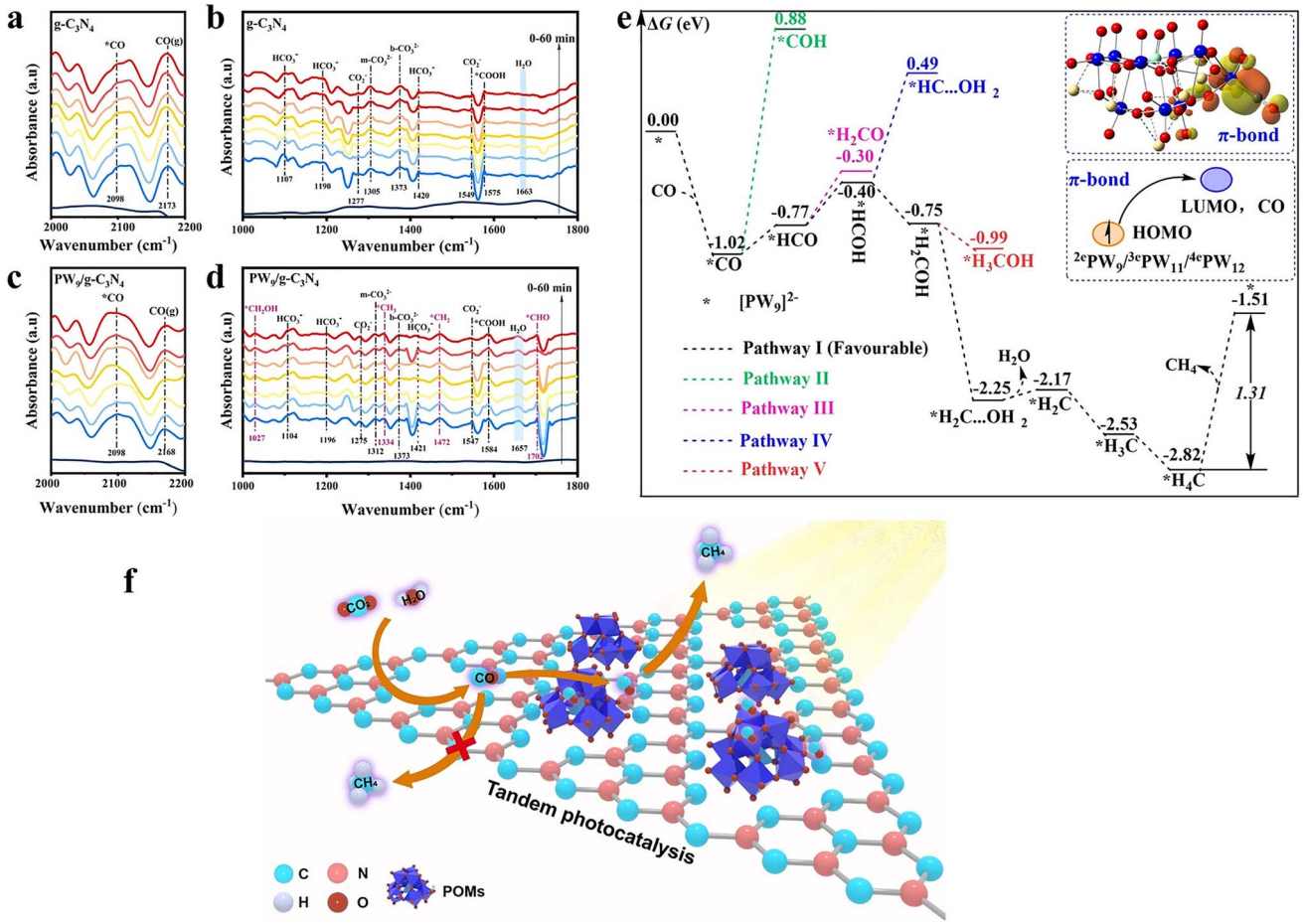

Fig. 9 *In situ* DRIFTS spectra during the photocatalytic CO_2 reduction process of (a) g-C_3N_4 in 2000–2200 cm^{-1}; (b) g-C_3N_4 in 1000–1800 cm^{-1}; (c) PW_9/g-C_3N_4 in the range of 2000–2200 cm^{-1} and (d) PW_9/g-C_3N_4 in the range of 1000–1800 cm^{-1}; (e) free energy change of CH_4 formation and release mediated by $[PW_9]^{2-}$ and the π-bond between W of $[PW_9]^{2-}$ and C of CO; and (f) the reaction mechanism from CO_2 to CH_4.[119]

problem to be solved. Therefore, the light absorption ability of POMs still needs to be further improved to meet the practical application requirements. Secondly, due to the poor selectivity of the reduction products, the CO_2 reduction products are usually mixtures, and it is still challenging to generate the target products with high selectivity and to separate the products (*e.g.*, methane and methanol). An in-depth study of the reaction mechanism is needed to improve the product selectivity by modulating the structure of POMs and reaction conditions. In addition, different strategies for different types of modified POMs can have different advantages and disadvantages. For example, when a POM is coated with a MOF, the reactants may have difficulty in accessing the active sites, and the selectivity may not be as good as that of homogeneous catalysts in some reactions. Some POM@MOF composites easily decompose under strongly acidic, strongly basic or high temperature conditions, which affects the catalytic performance. The MOF structure may collapse and the POM may be inactivated at high temperatures. Furthermore, POMs modified with g-C_3N_4 also face the disadvantages of a lack of catalytic centers and poor chemical stability. So, the stability and reusability of POM-based catalysts also need to be further optimised. Finally, for the photocatalytic reaction, none of the currently reported POM molecules can be separated from additional photosensitisers or sacrificial agents to maintain the catalytic reaction cycle, which has limited applicability to green chemistry itself. Therefore, the design and development of photocatalysts with high catalytic activity that are also green remains the key to promoting and accelerating the reaction process.

Looking ahead, the following research directions are worthy of attention: firstly, novel POMs can be designed and synthesised on POM bodies to modulate the energy band structure, redox potential and light absorption properties of POMs through the introduction of different metal elements, organic ligands or functional groups, so as to improve their photocatalytic activity. Secondly, to construct more efficient POM-based composites, it is essential to consider multiple strategies, such as combining POMs with semiconductors, metal–organic frameworks (MOFs), or carbon materials. These composites can form heterojunctions or synergistic catalytic systems to enhance light absorption, charge separation, and catalytic efficiency. In addition, efficient photocatalytic reactors can be

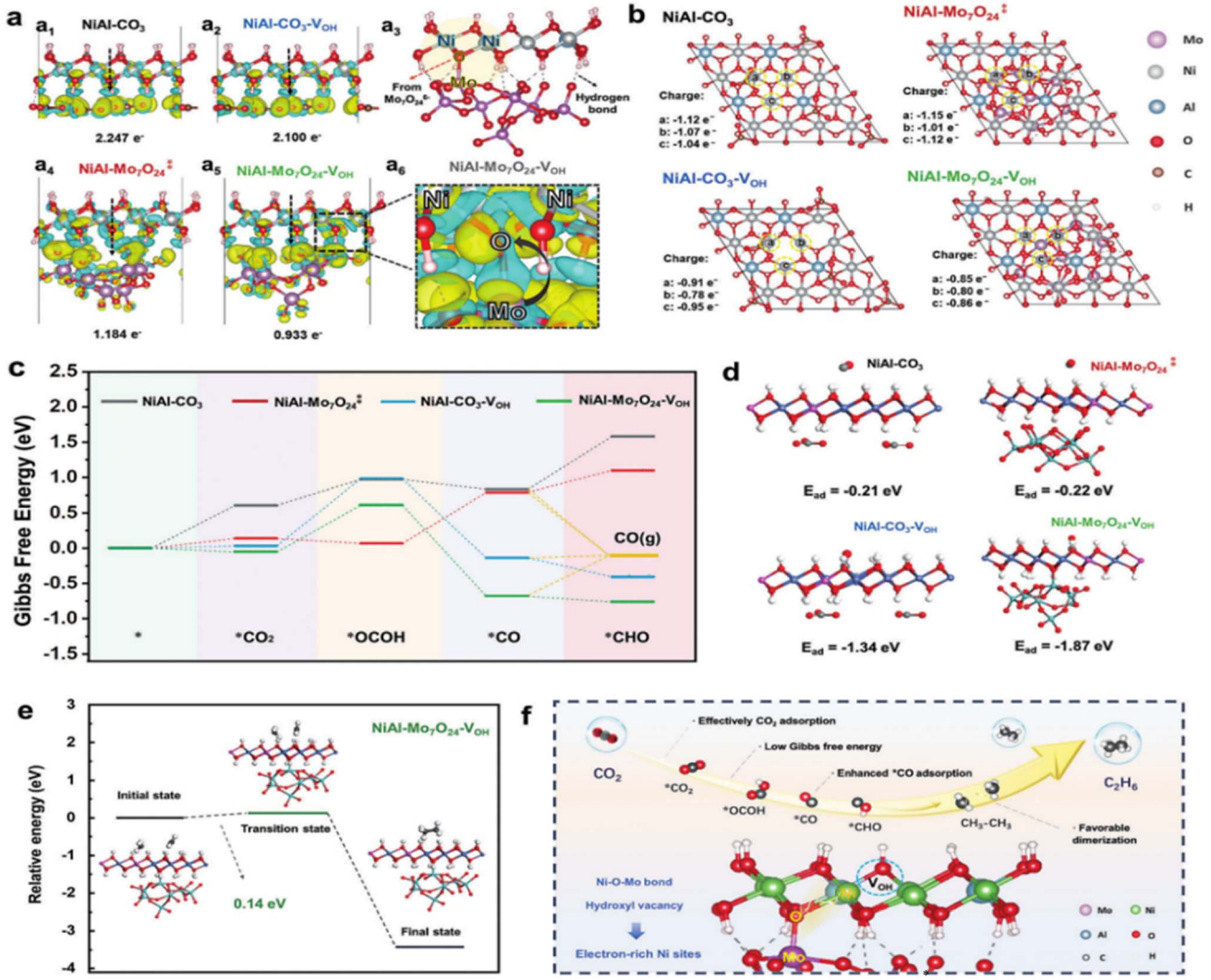

Fig. 10 (a) Differential charge density calculations for (a_1) NiAl–CO_3, (a_2) NiAl–CO_3–V_{OH} (a_4) NiAl – $Mo_7O_{24}^*$, (a_5), NiAl–Mo_7O_{24}–V_{OH} and (a_6) locally amplified spectra of NiAl–Mo_7O_{24}–V_{OH}; blue regions represent charge loss and yellow regions represent charge accumulation. (a_3) Structural diagram of NiAl–Mo_7O_{24}–V_{OH}. (b) Bader charge values of selected atoms in the crystal structure of NiAl–CO_3, NiAl – $Mo_7O_{24}^*$, NiAl–CO_3–V_{OH}, and NiAl–Mo_7O_{24}–V_{OH}. (c) Free energy diagrams of CO_2 photocatalytic reduction to CO/*CHO on NiAl–CO_3, NiAl – $Mo_7O_{24}^*$, NiAl–CO_3–V_{OH}, and NiAl–Mo_7O_{24}–V_{OH}. (d) The ball-and-stick structural models of the theoretical calculations of the adsorption energy of *CO on pristine NiAl–CO_3, NiAl – $Mo_7O_{24}^*$, NiAl–CO_3–V_{OH}, and NiAl–Mo_7O_{24}–V_{OH}. (e) Structures of the initial, transition, and final states, and the energy diagram for *CH_3 dimerization on NiAl–Mo_7O_{24}–V_{OH}. (f) Schematic illustration of the enhancement mechanism of CO_2 photoreduction to C_2H_6 *via* engineering electron-rich Ni active sites through the combination effect of hydroxyl vacancies and intercalated molybdate anions.[125]

developed to improve the efficiency of light utilisation and design efficient photocatalytic reactors. The contact between light, catalyst and reactants can be optimised to improve the photocatalytic reaction efficiency. Finally, theoretical calculations and experimental studies can be combined to explore the structure and reaction mechanism of POMs in depth using theoretical calculations in combination with more novel techniques such as *in situ* XAFS to guide experimental design and catalyst optimisation. To better expand the application scope of POMs in photocatalytic CO_2 reduction and explore their potential in other photocatalytic reactions, further research is needed.

Additionally, polyoxometalate (POM)-based materials exhibit broad application prospects in energy conversion, environmental remediation, and chemical synthesis due to their unique catalytic, photoelectric, and structurally tunable properties. Although laboratory studies have confirmed their excellent performance, the commercialization and industrialization of POM-based materials still face numerous challenges. To transition this technology from the lab to practical applications, a systematic evaluation of their commercial potential and the development of a rational industrialization pathway are essential.

The core advantages of POM-based materials lie in their high catalytic activity, structural designability, and potential for low-

cost production. For example, Keggin- or Dawson-type POMs can be optimized through heteroatom doping or organic–inorganic hybridization strategies to fine-tune their electronic structures, achieving high selectivity and stability in reactions such as CO_2 reduction and pollutant degradation. Moreover, the primary constituent elements of POMs (*e.g.*, W, Mo, and V) are abundant, and their synthesis processes are relatively mature, providing a foundation for large-scale production. However, industrial-scale adoption still requires addressing several key issues: first, ensuring uniformity and reproducibility in large-scale synthesis remains challenging, as traditional solvothermal methods often suffer from uneven mass transfer and reduced yields when scaled up. Second, the structural stability of POMs in continuous reactions is insufficient, particularly in liquid-phase systems where leaching or deactivation (*e.g.*, $H_3PW_{12}O_{40}$ loss in aqueous catalysis) and structural collapse can occur, necessitating immobilization on supports. Finally, real-world industrial applications demand far greater material quantities and poison resistance than laboratory testing conditions.

To overcome these bottlenecks, coordinated efforts are needed in material optimization, production processes, and application scenarios. At the material level, composite encapsulation (*e.g.*, POM@MOF and carbon-supported) or low-dimensional structuring (*e.g.*, nanosheets) can enhance stability and active site exposure while preventing component loss. In production processes, continuous-flow synthesis using microchannel reactors can replace batch synthesis to improve yield—for instance, Bayer's continuous-flow process increased production capacity tenfold. Additionally, green chemistry techniques (*e.g.*, solvent-free synthesis and microwave-assisted synthesis) can boost efficiency and reduce costs (*e.g.*, the University of Tokyo's solvent-free synthesis method). In terms of applications, POM-based materials could first penetrate high-value sectors (*e.g.*, pharmaceutical intermediate catalysis and high-end electronic chemicals) before expanding into large-scale markets like energy and environmental remediation. Leveraging carbon tax policies, integrated POM-based CO_2 capture-catalysis technologies (*e.g.*, the EU's 2020 project) could also be promoted. Furthermore, industry-academia collaboration and policy support are crucial, such as partnering with chemical companies to establish pilot production lines for material validation.

In summary, POM-based materials show short-term commercialization potential in niche fields like fine chemicals, medium-term expansion into energy storage and pollution control, and long-term prospects as a key carbon neutrality technology. Their successful industrialization depends not only on breakthroughs in material performance but also on collaborative innovation across the entire supply chain, ultimately enabling their transition from the laboratory to real-world industrial applications.

Finally, polyoxometalates have a broad application prospect in the areas of photocatalytic reduction of CO_2. By continuously overcoming challenges and exploring new research directions, we believe that highly efficient, stable and selective POM-based photocatalysts can be developed in the future, contributing to the goal of carbon neutrality.

Data availability

Data are available on request from the corresponding author.

Conflicts of interest

There are no conflicts to declare.

Acknowledgements

We gratefully acknowledge financial support from the "Grassland Talents" of Inner Mongolia Autonomous Region; Young Talents of Science and Technology in Universities of Inner Mongolia Autonomous Region (NJYT23030); Technology Breakthrough Engineering Hydrogen Energy Field "Unveiling and Leading" Project (2024KJTW0018); "Steed plan High level Talents" of Inner Mongolia University; Carbon Neutralization Research Project (STZX202218); National Natural Science Foundation of China (U22A20107); Inner Mongolia Autonomous Region Natural Science Foundation (2023MS02002); Guangdong Provincial Key Laboratory of Materials and Technologies for Energy Conversion (MATEC2024KF011); National Key R&D Program of China (2022YFA1205201).

References

1 H. L. Wu, X. B. Li, C. H. Tung and L. Z. Wu, *Adv. Mater.*, 2019, **31**, 1900709.
2 Y. Wei, J. Li, D. Zhao, Y. Zhao, Q. Zhang, L. Gu, J. Wan and D. Wang, *CCS Chem.*, 2024, **6**, 3065–3076.
3 M. Nyman and P. C. Burns, *Chem. Soc. Rev.*, 2012, **41**, 7354–7367.
4 H. Kumagai, Y. Tamaki and O. Ishitani, *Acc. Chem. Res.*, 2022, **55**, 978–990.
5 L. Qiu, S. Shen, C. Ma, C. Lv, X. Guo, H. Jiang, Z. Liu, W. Qiao, L. Ling and J. Wang, *Chem. Eng. J.*, 2022, **440**, 135956.
6 D. M. Koshy, S. S. Nathan, A. S. Asundi, A. M. Abdellah, S. M. Dull, D. A. Cullen, D. Higgins, Z. Bao, S. F. Bent and T. F. Jaramillo, *Angew. Chem., Int. Ed.*, 2021, **60**, 17472–17480.
7 Z. Fu, Q. Yang, Z. Liu, F. Chen, F. Yao, T. Xie, Y. Zhong, D. Wang, J. Li, X. Li and G. Zeng, *J. CO2 Util.*, 2019, **34**, 63–73.
8 X. Cui, Y. Sun and X. Xu, *Chin. Chem. Lett.*, 2023, **34**, 107348.
9 Z. Zeb, Y. Huang, L. Chen, W. Zhou, M. Liao, Y. Jiang, H. Li, L. Wang, L. Wang, H. Wang, T. Wei, D. Zang, Z. Fan and Y. Wei, *Coord. Chem. Rev.*, 2023, **482**, 215058.
10 B. Li, X. j. Liu, H. w. Zhu, H. p. Guan and R. t. Guo, *Small*, 2024, **20**, 2406074.
11 H. A. Maitlo, S. A. Younis, C. S. Lee and K.-H. Kim, *Adv. Colloid Interface Sci.*, 2025, **341**, 103483.

12 Y. A. Alli, N. E. Magida, F. Matebese, N. Romero, A. S. Ogunlaja and K. Philippot, *Mater. Today Energy*, 2023, **34**, 101310.
13 H. S. Shafaat and J. Y. Yang, *Nat. Catal.*, 2021, **4**, 928–933.
14 Z. Wang, Y. Hu, S. Zhang and Y. Sun, *Chem. Soc. Rev.*, 2022, **51**, 6704–6737.
15 E. Sivasurya, R. Atchudan, M. G. Mohamed, A. Thangamani, S. Rajendran, A. Jalil, P. K. Kalambate, D. Manoj and S.-W. Kuo, *Mater. Today Chem.*, 2025, **44**, 102538.
16 K. Zhang, X. Wang, H. Li, X. Zhao, G. Zhang, C. Tan, Y. Wang and B. Li, *Appl. Energy*, 2025, **377**, 124408.
17 D. Li, M. Kassymova, X. Cai, S.-Q. Zang and H.-L. Jiang, *Coord. Chem. Rev.*, 2020, **412**, 213262.
18 J. Lin, J. He, Q. Huang, Y. Luo, Y. Zhang, W. Li, G. Zhou, J. Hu, Z. Yang and Y. Zhou, *Appl. Catal. B Environ. Energy*, 2025, **362**, 124747.
19 X. J. Kong, Z. Lin, Z. M. Zhang, T. Zhang and W. Lin, *Angew. Chem., Int. Ed.*, 2016, **55**, 6411–6416.
20 N. Li, J. Liu, B. X. Dong and Y. Q. Lan, *Angew. Chem., Int. Ed.*, 2020, **59**, 20779–20793.
21 M. Lu, M. Zhang, J. Liu, T.-Y. Yu, J.-N. Chang, L.-J. Shang, S.-L. Li and Y.-Q. Lan, *J. Am. Chem. Soc.*, 2022, **144**, 1861–1871.
22 J. Gu, W. Chen, G. G. Shan, G. Li, C. Sun, X. L. Wang and Z. Su, *Mater. Today Energy*, 2021, **21**, 100760.
23 F. Xing, R. Zeng, C. Cheng, Q. Liu and C. Huang, *Appl. Catal., B*, 2022, **306**, 121087.
24 C. Boskovic, *Acc. Chem. Res.*, 2017, **50**, 2205–2214.
25 Y. Zhou, K. Wang, S. Zheng, X. Cheng, Y. He, W. Qin, X. Zhang, H. Chang, N. Zhong and X. He, *Chem. Eng. J.*, 2024, **486**, 150169.
26 C. Liu, Y. Wu, K. Sun, J. Fang, A. Huang, Y. Pan, W.-C. Cheong, Z. Zhuang, Z. Zhuang, Q. Yuan, H. L. Xin, C. Zhang, J. Zhang, H. Xiao, C. Chen and Y. Li, *Chem*, 2021, **7**, 1297–1307.
27 M. Jun, C. Kwak, S. Y. Lee, J. Joo, J. M. Kim, D. J. Im, M. K. Cho, H. Baik, Y. J. Hwang, H. Kim and K. Lee, *Small Methods*, 2022, **6**, 220007.
28 L. Wang, L. Wang, S. Yuan, L. Song, H. Ren, Y. Xu, M. He, Y. Zhang, H. Wang, Y. Huang, T. Wei, J. Zhang, Y. Himeda and Z. Fan, *Appl. Catal., B*, 2023, **322**, 122097.
29 S. Bai, N. Zhang, C. Gao and Y. Xiong, *Nano Energy*, 2018, **53**, 296–336.
30 L. Liu, S. Wang, H. Huang, Y. Zhang and T. Ma, *Nano Energy*, 2020, **75**, 104959.
31 W. Tu, Y. Zhou and Z. Zou, *Adv. Mater.*, 2014, **26**, 4607–4626.
32 A. L. Linsebigler, G. Lu and J. T. Yates, *Chem. Rev.*, 1995, **95**, 735–758.
33 M. Mikkelsen, M. Jørgensen and F. C. Krebs, *Energy Environ. Sci.*, 2010, **3**, 43–81.
34 Y. Dong, Q. Han, Q. Hu, C. Xu, C. Dong, Y. Peng, Y. Ding and Y. Lan, *Appl. Catal., B*, 2021, **293**, 120214.
35 Z. Wang, G. Zou, J. H. Park and K. Zhang, *Sci. China Mater.*, 2024, **67**, 397–423.
36 X. Tao, Y. Zhao, S. Wang, C. Li and R. Li, *Chem. Soc. Rev.*, 2022, **51**, 3561–3608.
37 H. Shen, M. Yang, L. Hao, J. Wang, J. Strunk and Z. Sun, *Nano Res.*, 2021, **15**, 2773–2809.
38 S. Yue, Z. Zhao, T. Zhang, P. Wang and S. Zhan, *Mater. Today Energy*, 2024, **40**, 101482.
39 S. Yang, W. J. Byun, F. Zhao, D. Chen, J. Mao, W. Zhang, J. Peng, C. Liu, Y. Pan, J. Hu, J. Zhu, X. Zheng, H. Fu, M. Yuan, H. Chen, R. Li, M. Zhou, W. Che, J. B. Baek, J. S. Lee and J. Xu, *Adv. Mater.*, 2024, **36**, 2312616.
40 R. Yang, Y. Fan, Y. Zhang, L. Mei, R. Zhu, J. Qin, J. Hu, Z. Chen, Y. Hau Ng, D. Voiry, S. Li, Q. Lu, Q. Wang, J. C. Yu and Z. Zeng, *Angew. Chem., Int. Ed.*, 2023, **62**, e202218016.
41 X. Jiao, K. Zheng, L. Liang, X. Li, Y. Sun and Y. Xie, *Chem. Soc. Rev.*, 2020, **49**, 6592–6604.
42 H. N. Miras, J. Yan, D.-L. Long and L. Cronin, *Chem. Soc. Rev.*, 2012, **41**, 7403–7430.
43 D.-Y. Du, J.-S. Qin, S.-L. Li, Z.-M. Su and Y.-Q. Lan, *Chem. Soc. Rev.*, 2014, **43**, 4615–4632.
44 Y. Luo, C. Zhang, B. Zheng, X. Geng and M. Debliquy, *Int. J. Hydrogen Energy*, 2017, **42**, 20386–20397.
45 S. Mahajan and S. Jagtap, *Appl. Mater. Today*, 2020, **18**, 100483.
46 A. W. Morawski, M. Gano, K. Ćmielewska, E. Kusiak-Nejman, I. Pełech, P. Staciwa, E. Ekiert and U. Narkiewicz, *Catalysts*, 2023, **13**, 1270.
47 H.-Y. Xu, S.-Q. Zhang, Y.-F. Wang, Y. Xu, L.-M. Dong and S. Komarneni, *Appl. Surf. Sci.*, 2023, **614**, 156225.
48 S. Bai, W. Jing, G. He, C. Liao, F. Wang, Y. Liu and L. Guo, *ACS Nano*, 2023, **17**, 10976–10986.
49 X. Liu, T. Zhang, Y. Li, J. Zhang, Y. Du, Y. Yang, Y. Jiang and K. Lin, *Chem. Eng. J.*, 2022, **434**, 134602.
50 W. Cai, Z. Qian, C. Hu, W. Zheng, L. Luo and Y. Zhao, *Chem. Eng. J.*, 2024, **479**, 147718.
51 S. Khan, V. Poliukhova, N. Tamir, J. Park, N. Suzuki, C. Terashima, K.-I. Katsumata and S.-H. Cho, *Int. J. Hydrogen Energy*, 2023, **48**, 9713–9722.
52 Y. Rambabu, U. Kumar, N. Singhal, M. Kaushal, M. Jaiswal, S. L. Jain and S. C. Roy, *Appl. Surf. Sci.*, 2019, **485**, 48–55.
53 Y. Chen, W. Zhong, F. Chen, P. Wang, J. Fan and H. Yu, *J. Mater. Sci. Technol.*, 2022, **121**, 19–27.
54 H. Wang, *Nano Res.*, 2021, **15**, 2834–2854.
55 H. Huang, Q. Lin, Q. Niu, J. Ning, L. Li, J. Bi and Y. Yu, *Chin. J. Catal.*, 2024, **60**, 201–208.
56 L. Zhang, L. Mei, K. Wang, Y. Lv, S. Zhang, Y. Lian, X. Liu, Z. Ma, G. Xiao, Q. Liu, S. Zhai, S. Zhang, G. Liu, L. Yuan, B. Guo, Z. Chen, K. Wei, A. Liu, S. Yue, G. Niu, X. Pan, J. Sun, Y. Hua, W.-Q. Wu, D. Di, B. Zhao, J. Tian, Z. Wang, Y. Yang, L. Chu, M. Yuan, H. Zeng, H.-L. Yip, K. Yan, W. Xu, L. Zhu, W. Zhang, G. Xing, F. Gao and L. Ding, *Nano-Micro Lett.*, 2023, **15**, 177.
57 W. Huang, Q. Zhu, Y. Zhu, C. Chen and J. Shen, *Mater. Today Energy*, 2023, **38**, 101458.
58 Z. Lang, J. Miao, Y. Lan, J. Cheng, X. Xu and C. Cheng, *APL Mater.*, 2020, **8**, 120702.
59 Y. Cao, Q. Chen, C. Shen and L. He, *Molecules*, 2019, **24**, 2069.

60 Q. Hu, S. Chen, T. Wågberg, H. Zhou, S. Li, Y. Li, Y. Tan, W. Hu, Y. Ding and X. Han, *Angew. Chem., Int. Ed.*, 2023, **62**, 2–10.
61 A. Panagiotopoulos, A. M. Douvas, P. Argitis and A. G. Coutsolelos, *ChemSusChem*, 2016, **9**, 3213–3219.
62 S. B. Yu, Q. Qi, B. Yang, H. Wang, D. W. Zhang, Y. Liu and Z. T. Li, *Small*, 2018, **14**, 1801037.
63 B.-L. Fei, J.-K. Zhong, N.-P. Deng, J.-H. Wang, Q.-B. Liu, Y.-G. Li and X. Mei, *Chemosphere*, 2018, **197**, 241–250.
64 R.-L. Liu, Y. Chen, X. Su, W. Zhu, Z. Liu, Y. Chen, D.-Y. Wang and G. Li, *Coord. Chem. Rev.*, 2025, **522**, 216224.
65 C. Dey, *Coord. Chem. Rev.*, 2024, **510**, 215847.
66 J. Liang, M. Wu, L. Qi, S. Qian, H. Rui, Y. Liu and C. Liu, *Fuel*, 2024, **360**, 130597.
67 K. Li, Y. Liu, G. Yang, Z. Zheng, X. Lin, Z. Zhang, S. Li, Y. Liu and Y. Wei, *Green Chem.*, 2024, **26**, 6454–6460.
68 G. Murmu, S. Samajdar, S. Ghosh, K. Shakeela and S. Saha, *Chemosphere*, 2024, **346**, 140576.
69 D. Li, P. Ma, J. Niu and J. Wang, *Coord. Chem. Rev.*, 2019, **392**, 49–80.
70 I.-M. Mbomekalle, Y. W. Lu, B. Keita and L. Nadjo, *Inorg. Chem. Commun.*, 2004, **7**, 86–90.
71 C. R. Graham and R. G. Finke, *Inorg. Chem.*, 2008, **47**, 3679–3686.
72 K. Nomiya, T. Shirai and M. Miwa, *Polyhedron*, 1986, **6**, 213–218.
73 T. J. R. Weakley and L. C. W. Baker, *J. Inorg. Nucl. Chem.*, 1966, **28**, 447–454.
74 L. C. W. Baker, G. A. Gallagher and T. P. McCutcheon, *J. Am. Chem. Soc.*, 1953, **75**, 10.
75 Y. W. Lu, B. Keita, L. Nadjo, G. Lagarde, E. Simoni, G. Zhang and G. A. Tsirlina, *J. Phys. Chem. B*, 2006, **110**, 15633–15639.
76 T. M. A. Bakker, S. Mathew and J. N. H. Reek, *Sustain. Energy Fuels*, 2019, **3**, 96–100.
77 X. Huang and X. Liu, *Appl. Surf. Sci.*, 2020, **505**, 144527.
78 S.-S. Wang, S.-Y. Feng, Z.-Y. Rong, X.-Y. Wu, W. Wu and C.-Z. Lu, *Inorg. Chem.*, 2025, **64**, 3256–3265.
79 Y. Gao, F. Yang, Y. Wang, A. P. R. Johnston, R. N. Duffin, P. C. Andrews, C. Ritchie and G. K. Such, *Chem. Sci.*, 2025, **16**, 288–296.
80 L. Qiao, M. Song, A. Geng and S. Yao, *Chin. Chem. Lett.*, 2019, **30**, 1273–1276.
81 K. Talbi, F. Penas-Hidalgo, A. L. Robinson, P. Gotico, W. Leibl, P. Mialane, M. Gomez-Mingot, M. Fontecave, A. Solé-Daura, C. Mellot-Draznieks and A. Dolbecq, *Appl. Catal. B Environ. Energy*, 2024, **345**, 123681.
82 A. M. Khenkin, I. Efremenko, L. Weiner, J. M. L. Martin and R. Neumann, *Chem.–Eur. J.*, 2010, **16**, 1356–1364.
83 B. Li, M. Chen, Q. Hu, J. Zhu, X. Yang, Z. Li, C. Hu, Y. Li, P. Ni and Y. Ding, *Appl. Catal. B Environ. Energy*, 2024, **346**, 123733.
84 S. Barman, S. S. Sreejith, S. Garai, R. Pochamoni and S. Roy, *ChemPhotoChem*, 2018, **3**, 93–100.
85 Y. Ma, H. Peng, J. Liu, Y. Wang, X. Hao, X. Feng, S. U. Khan, H. Tan and Y. Li, *Inorg. Chem.*, 2018, **57**, 4109–4116.
86 D. Chai, C. J. Gómez-García, B. Li, H. Pang, H. Ma, X. Wang and L. Tan, *Chem. Eng. J.*, 2019, **373**, 587–597.
87 X. Zhao, S. Zhang, J. Yan, L. Li, G. Wu, W. Shi, G. Yang, N. Guan and P. Cheng, *Inorg. Chem.*, 2018, **57**, 5030–5037.
88 B.-Y. Zhang, X.-S. Wu, N.-H. Wang, X.-L. Wang, X.-Q. Han and Z.-M. Su, *Chem. Eng. J.*, 2024, **500**, 157502.
89 Z. Zhang, J. Ran, E. Fan, S. Zhou, D.-F. Chai, W. Zhang, M. Zhao and G. Dong, *J. Alloys Compd.*, 2023, **968**, 172169.
90 X.-X. Li, J. Liu, L. Zhang, L.-Z. Dong, Z.-F. Xin, S.-L. Li, X.-Q. Huang-Fu, K. Huang and Y.-Q. Lan, *ACS Appl. Mater. Interfaces*, 2019, **11**, 25790–25795.
91 S.-Q. You, Y.-J. Dong, B.-S. Hou, M. Dong, J.-L. Tong, L.-X. Wang, X.-L. Wang, C.-Y. Sun, W. Guan and Z.-M. Su, *J. Mater. Chem. C*, 2023, **11**, 7389–7396.
92 Z. Wang, T. Wang, Y. Zhao, Q. Ye and P. He, *J. Catal.*, 2025, **442**, 115908.
93 H. Li, M. Chi, X. Xin, R. Wang, T. Liu, H. Lv and G.-Y. Yang, *Chin. J. Catal.*, 2023, **50**, 343–351.
94 F. Wang, X. Tian, Y. Shi, W. Fan and Q. Liu, *Int. J. Hydrogen Energy*, 2024, **68**, 1382–1392.
95 M. M. Kandy and V. G. Gaikar, *Mater. Res. Bull.*, 2018, **102**, 440–449.
96 F. Meng, C. Qu, L. Wang, D. Yang, Z. Zhao and Q. Ye, *J. Colloid Interface Sci.*, 2025, **684**, 492–502.
97 F. Si, G. Wang, M. Lv, J. Bai, Y. Li, T. Hou and Y. Li, *Appl. Catal. B Environ. Energy*, 2025, **365**, 124934.
98 F. Duan, X. Liu, D. Qu, B. Li and L. Wu, *CCS Chem.*, 2021, **3**, 2676–2687.
99 C. Li, S. Dong, R. Tang, X. Ge, Z. Zhang, C. Wang, Y. Lu and L. Yin, *Energy Environ. Sci.*, 2018, **11**, 3201–3211.
100 L. Zeng, X. Guo, C. He and C. Duan, *ACS Catal.*, 2016, **6**, 7935–7947.
101 J. Dhainaut, M. Bonneau, R. Ueoka, K. Kanamori and S. Furukawa, *ACS Appl. Mater. Interfaces*, 2020, **12**, 10983–10992.
102 P. D. Morris, I. J. McPherson, M. A. Edwards, R. J. Kashtiban, R. I. Walton and P. R. Unwin, *Angew. Chem., Int. Ed.*, 2020, **59**, 19696–19701.
103 N. Stock and S. Biswas, *Chem. Rev.*, 2011, **112**, 933–969.
104 Z. Hu, B. J. Deibert and J. Li, *Chem. Soc. Rev.*, 2014, **43**, 5815–5840.
105 Y.-R. Wang, Q. Huang, C.-T. He, Y. Chen, J. Liu, F.-C. Shen and Y.-Q. Lan, *Nat. Commun.*, 2018, **9**, 4466.
106 Y. Benseghir, A. Lemarchand, M. Duguet, P. Mialane, M. Gomez-Mingot, C. Roch-Marchal, T. Pino, M.-H. Ha-Thi, M. Haouas, M. Fontecave, A. Dolbecq, C. Sassoye and C. Mellot-Draznieks, *J. Am. Chem. Soc.*, 2020, **142**, 9428–9438.
107 P. Mialane, C. Mellot-Draznieks, P. Gairola, M. Duguet, Y. Benseghir, O. Oms and A. Dolbecq, *Chem. Soc. Rev.*, 2021, **50**, 6152–6220.
108 M. Samaniyan, M. Mirzaei, R. Khajavian, H. Eshtiagh-Hosseini and C. Streb, *ACS Catal.*, 2019, **9**, 10174–10191.
109 J. Du, Y. Ma, X. Xin, H. Na, Y. Zhao, H. Tan, Z. Han, Y. Li and Z. Kang, *Chem. Eng. J.*, 2020, **398**, 125518.
110 C. Gao, J. Wang, H. Xu and Y. Xiong, *Chem. Soc. Rev.*, 2017, **46**, 2799–2823.
111 J. Du, Y.-Y. Ma, W.-J. Cui, S.-M. Zhang, Z.-G. Han, R.-H. Li, X.-Q. Han, W. Guan, Y.-H. Wang, Y.-Q. Li, Y. Liu, F.-Y. Yu,

K.-Q. Wei, H.-Q. Tan, Z.-H. Kang and Y.-G. Li, *Appl. Catal., B*, 2022, **318**, 121812.
112 Y. Zhao, D. Yang, C. Yu and H. Yan, *J. Environ. Chem. Eng.*, 2025, **13**, 115348.
113 J. Zhang, Y. Chen and X. Wang, *Energy Environ. Sci.*, 2015, **8**, 3092–3108.
114 Y. Wang, X. Wang and M. Antonietti, *Angew. Chem., Int. Ed.*, 2011, **51**, 68–89.
115 X. Gao, B. Yang, W. Yao, Y. Wang, R. Zong, J. Wang, X. Li, W. Jin and D. Tao, *Environ. Pollut.*, 2020, **257**, 113577.
116 O. P. Nagar, T. Barman, K. Marumoto, Y. Shimoi, K. Matsuishi and N. Chouhan, *Int. J. Hydrogen Energy*, 2024, **87**, 526–538.
117 J. Wang, H. Cheng, D. Wei and Z. Li, *Chin. J. Catal.*, 2022, **43**, 2606–2614.
118 J. Zhou, W. Chen, C. Sun, L. Han, C. Qin, M. Chen, X. Wang, E. Wang and Z. Su, *ACS Appl. Mater. Interfaces*, 2017, **9**, 11689–11695.
119 Q. Zhu, Z. Li, T. Zheng, X. Zheng, S. Liu, S. Gao, X. Fu, X. Su, Y. Zhu, Y. Zhang and Y. Wei, *Angew. Chem., Int. Ed.*, 2024, **64**, e202413594.
120 Y. Tokudome, M. Fukui, S. Iguchi, Y. Hasegawa, K. Teramura, T. Tanaka, M. Takemoto, R. Katsura and M. Takahashi, *J. Mater. Chem. A*, 2018, **6**, 9684–9690.
121 Z. Gao, J. Liang, J. Yao, Y. zhao, Q. Meng, G. He and H. Chen, *J. Environ. Chem. Eng.*, 2021, **9**, 105405.
122 G. Mishra, B. Dash, S. Pandey and D. Sethi, *Appl. Clay Sci.*, 2018, **165**, 214–222.
123 A. Ghiasi Moaser, A. G. Afkham, R. Khoshnavazi and S. Rostamnia, *Sci. Rep.*, 2023, **13**, 4114.
124 X. Zhao, H. Jiang, Y. Xiao and M. Zhong, *Nanoscale Adv.*, 2024, **6**, 1241–1245.
125 C. Xu, S. Yu, M. Zhang, X. Zhan, S. Jiang, S. Wang, G. Liu, J. Ren, X. Sun, Y. Wang, H. Q. Peng, B. Liu, W. Zhang and Y. F. Song, *Adv. Funct. Mater.*, 2024, **35**, 2414893.
126 H. Nijs, M. D. Bock and E. F. Vansant, *J. Porous Mater.*, 1999, **6**, 101–110.
127 V. Rives and M. a. Angeles Ulibarri, *Coord. Chem. Rev.*, 1999, **181**, 61–120.
128 K.-H. Goh, T.-T. Lim and Z. Dong, *Water Res.*, 2008, **42**, 1343–1368.
129 Q. Wang and D. O'Hare, *Chem. Rev.*, 2012, **112**, 4124–4155.
130 R. Ma and T. Sasaki, *Adv. Mater.*, 2010, **22**, 5082–5104.
131 J. L. Gunjakar, T. W. Kim, H. N. Kim, I. Y. Kim and S.-J. Hwang, *J. Am. Chem. Soc.*, 2011, **133**, 14998–15007.
132 M. Xu, B. Bi, B. Xu, Z. Sun and L. Xu, *Appl. Clay Sci.*, 2018, **157**, 86–91.
133 J.-C. Liu, B. Qi and Y.-F. Song, *Dalton Trans.*, 2020, **49**, 3934–3941.